1.0 General

HAYNES 230 alloy is an austenitic Ni-Cr alloy that is solid-solution strengthened by additions of tungsten and molybdenum. In addition, the precipitation of chromium-rich $M_{23}C_6$ carbides on glide dislocations enhances the high temperature creep strength of the alloy. The alloy possesses excellent resistance to oxidizing environments at temperatures up to 2100F due to its high chromium content in combination with the minor elements silicon, manganese and lanthanum. Its low coefficient of thermal expansion provides the alloy with excellent resistance to thermal fatigue. The alloy has a balanced composition that avoids the formation of intermetallic phases such as sigma, mu or laves phases that could significantly reduce the ductility of the alloy. The alloy retains high levels of ductility and toughness following long term exposures in the 1200–1600F range. This leads to good resistance to thermal fatigue after long service exposures and good repairability characteristics. The microstructure consists of a face-centered cubic matrix and a large number of primary, tungsten-rich, M_6C carbides which control grain size and constrain grain growth when the alloy is exposed to very high temperatures for prolonged periods of time. Due to its high nickel content, the alloy also possesses good resistance to carburizing and nitriding environments. The alloy was commercialized in 1984 for high temperature components requiring excellent creep strength and oxidation resistance. Primary applications include combustors, transition ducts and temperature sensors in gas turbine engines and nozzles for rocket engines. Other applications include catalyst grid supports for the oxidation of ammonia for the manufacture of nitric acid, high temperature heat exchangers, high temperature bellows, heat treating equipment, and furnace retorts. The alloy is currently being evaluated for interconnects in solid oxide fuel cells, components for high temperature gas-cooled nuclear reactors, and components for ultrasupercritical steam power plants. (Ref. 1)

1.1 Commercial Designation

HAYNES 230 alloy

1.2 Alternate Designation

UNS N06230

1.3 Specifications

1.3.1 *[Table]* HAYNES 230 alloy: AMS and ASTM specifications

1.4 Composition

1.4.1 *[Table]* HAYNES 230 alloy: AMS specification limits

1.5 Heat Treatment

HAYNES 230 alloy is supplied in the solution heat-treated condition unless otherwise specified. The alloy is solution heat treated in the temperature range of 2150F to 2250F and rapidly cooled or water quenched for optimum properties. Annealing the alloy at lower temperatures will result in carbide precipitation which may marginally affect the alloy's strength and ductility. (Ref. 2)

	Ni
22.0	Cr
14.0	W
2.0	Mo
0.65	Mn
0.5	Si
0.35	Al
0.1	C
0.0275	La

1.6 Hardness

1.6.1 *[Table]* HAYNES 230 alloy: Hardness of various product forms

1.6.2 *[Table]* HAYNES 230 alloy: Hardness after imposed coldwork

1.7 Forms and Conditions Available

HAYNES 230 alloy is available in the forms of sheet, strip, foil, plate, bar, billet, wire, pipe and tubing. It is furnished in the solution heat treated condition. (Ref. 2)

1.8 Melting and Casting Practice

HAYNES 230 alloy is normally primary melted in air using an electric arc furnace plus argon oxygen decarburization practice. The hot metal is then cast into round or rectangular electrode molds depending on the product form required. The electrodes are then electroslag remelted to produce the final ingots.

1.9 Hydrogen Embrittlement Resistance

1.9.1 *[Table]* HAYNES 230 alloy: Hydrogen embrittlement resistance

In the solution-annealed condition, HAYNES 230 alloy is not subject to hydrogen embrittlement when exposed under isothermal conditions. However, if it is sensitized by an exposure at 1200F, then tested at 70F, the alloy becomes susceptible to hydrogen embrittlement and exhibits a notched tensile strength ratio of 0.41. (Ref. 7)

2.0 Physical Properties and Environmental Effects

2.1 Thermal Properties

2.1.1 Melting Range: 2375–2500F (Ref. 2)

2.1.2 Phase Changes

HAYNES 230 alloy was formulated using an electron valency, (N_v), control to avoid the formation of topologically closed-packed (TCP) phases such as sigma, mu, or Laves phases. In the studies carried out to date, none of these phases has been identified in samples given long-term exposures in the 1200–1800F temperature range. At temperatures below about 2100F, chromium-rich $M_{23}C_6$-type carbides have been observed to precipitate on grain and twin boundaries as well as on pre-existing dislocations. Based on alloy chemistry, these carbides are expected to be of the form $Cr_{21}(W, Mo)_2(C, B)_6$. If the alloy is given extended exposures in the 842–1022F (450–550C) temperature range, long range ordering to a Ni_2Cr-type compound has been indicated. Such an ordering reaction can also be anticipated by the discontinuity that occurs in the specific heat of the alloy in that temperature range. The long range ordering reaction results in a contraction of the alloy dimensions as shown in Table 2.1.2.1. (Refs. 1, 8–10)

2.1.2.1 *[Table]* HAYNES 230 alloy: Maximum shrinkage after 3000–hour exposures in the 842–1022F (450–550C) temperature range

2.1.3 Thermal Conductivity

2.1.3.1 *[Figure]* HAYNES 230 alloy: Thermal conductivity

2.1.4 Thermal Expansion

2.1.4.1 *[Figure]* HAYNES 230 alloy: Mean coefficient of thermal expansion

2.1.5 Specific Heat

2.1.5.1 *[Figure]* HAYNES 230 alloy: Specific heat

2.1.6 Thermal Diffusivity

2.1.6.1 *[Figure]* HAYNES 230 alloy: Thermal diffusivity

2.2 Other Physical Properties

2.2.1 Density: 0.324 lb/in^2 (8.97 g/cm^3) (Ref. 2)

2.2.2 Electrical Properties

2.2.2.1 *[Figure]* HAYNES 230 alloy: Electrical resistivity

2.2.3 Magnetic Properties

The magnetic properties of HAYNES 230 alloy have not been reported. However, based on its composition, the alloy can be probably described as very weakly paramagnetic. It is expected that its room temperature magnetic permeability would be similar to that of HASTELLOY X alloy which has a magnetic permeability of 1.002 at 200 oersteds (15,900 A/m). (Ref. 13)

2.2.4 Emittance

The spectral emittance of HAYNES 230 alloy was determined over the wavelength range of 0.8 to 20 µm at temperatures of 783–1751F (417–955C). The emittance values obtained were found to increase with temperature as the result of the development of nickel-chromium oxides on the surface of the alloy. The average values were on the order of 0.4 at 783F (417C) and 0.85 at 1751F (955C). The emittance stabilized at the highest temperature due to the formation of an opaque oxide layer and did not change during a subsequent cooling cycle. The total hemispherical emittance properties of the alloy were studied as part of a program to develop coatings with enhanced emissivity for thermophotovoltaic radiator applications. The measurements of emittance were made at room temperature and then extrapolated to 2012F (1100C). The emittance of the alloy substrate was measured uncoated and after annealing at 2012F (1100C)/500 hours in a vacuum (<10^{-5} torr). The emittance values obtained for the uncoated and annealed samples were 0.23 and 0.67, respectively. A large variety of coatings were studied, and emittance values as high as 0.85 were obtained. (Refs. 11, 12)

2.2.5 Damping Capacity

2.3 Chemical Environments

2.3.1 General Corrosion

2.3.1.1 *[Table]* Aqueous corrosion resistance for several nickel-base alloys

HAYNES 230 alloy has excellent resistance to dilute nitric and sulfuric acids, but its resistance to dilute hydrochloric acid is poor.

2.3.2 Stress Corrosion

Triplicate u-bend samples of HAYNES 230 alloy were tested in boiling $MgCl_2$, and no evidence of chloride stress corrosion cracking was observed after 1008 hours. (Ref. 14)

2.3.3 Oxidation Resistance

HAYNES 230 alloy has been found to be the most oxidation resistant alloy among those alloys that depend on the formation of chromium oxides for protection. Its excellent oxidation resistance derives from the formation of a $Mn_{1.5}Cr_{1.5}O_4$ spinel oxide outer layer on top of a Cr_2O_3 inner layer. The use of minor additions of Si and La reduce the tendency of these oxides to spall during thermal cycling. Oxidation attack tends to be greater in flowing air due to the volitization of chromium oxide. Short-term oxidation data is often useful to rank the performance of various alloys. However, it does not indicate whether or not an alloy is subject to a phenomenon known as breakaway oxidation. (Refs. 16, 17)

Burner rig oxidation is much more aggressive due to the high velocity combustion gas stream and a much shorter thermal cycle. The samples were exposed to combustion gases of No. 2 fuel oil burned at a ratio of 50:1 air to fuel. This produced a combustion gas velocity of about 0.3 mach. The samples were automatically cycled out of the combustion gas stream and fan cooled to near ambient temperature every 30 minutes, then reinserted into the flame tunnel. (Table 2.3.3.4)

2.3.3.1 *[Table]* Short-term oxidation in flowing air for several nickel-base alloys

2.3.3.2 *[Table]* Long-term oxidation in still air for several nickel-base alloys

2.3.3.3 *[Table]* Long-term oxidation in flowing air for several nickel-base alloys

2.3.3.4 *[Table]* Burner rig oxidation resistance at 1800F (982C) for 1000 hours for several nickel-base alloys

2.3.4 Hot Corrosion

HAYNES 230 alloy has excellent resistance to $NaSO_4$-induced hot corrosion attack in spite of the fact that it is a nickel-base alloy. The level of attack generally tends to increase with the level of salt injected. However, 230 and 188 alloys demonstrate excellent resistance at both levels due to their more protective oxide scales. (Ref. 18)

2.3.4.1 *[Table]* Hot corrosion resistance at 1650F (900C) for several nickel-base alloys

2.3.5 Nitriding Resistance

2.3.5.1 *[Table]* Nitrogen absorption in flowing NH_3 after 168 hours for several nickel-base alloys

Due to its high nickel content, HAYNES 230 alloy has excellent resistance to high temperature nitriding environments. Pure nitrogen tends to be more aggressive than ammonia. (Refs. 2, 19)

2.3.5.2 *[Table]* Nitrogen absorption and internal penetration in N_2 at 2000F (1093C) for 168 hours for several nickel-base alloys

Since combustion gas environments using air as the source of oxygen contain a large amount of nitrogen, nitridation can be an important problem if the protective oxides spall. The oxides formed on HAYNES 230 alloy resist spallation, and very little nitridation is observed. The nitrogen pick-up is also greater in alloys containing aluminum such as 263 and 617 alloys, or those containing large amounts of iron such as X alloy. (Ref. 20)

2.3.5.3 *[Table]* Nitrogen pick-up following burner rig testing at 1800F (980C) for 1000 hours with 30-minute cycling for several nickel-base alloys

2.3.6 Metal Dusting Resistance

Due its high nickel and chromium contents along with its low iron content, HAYNES 230 alloy has reasonably good resistance to metal dusting. A study carried out at 1100F (593C) in a gas environment with a carbon activity of 104 and a pressure of 1 atm. revealed that the alloy suffered no weight loss after 14,000 hours of exposure. (Refs. 21, 22)

2.3.6.1 *[Table]* Final metal wastage rates in a gas with a carbon activity of 18.9 at 1200F (650C) and 1 atm pressure for several nickel-base alloys

3.0 Mechanical Properties

3.1 Specified Mechanical Properties

3.1.1 AMS and ASTM Specifications

3.1.1.1 *[Table]* HAYNES 230 alloy: Room temperature tensile requirements

3.1.1.2 *[Table]* HAYNES 230 alloy: Stress rupture requirements for AMS specifications

3.2 Mechanical Properties at Room Temperature

3.2.1 Tension Stress-Strain Diagrams and Tensile Properties

3.2.1.1 *[Figure]* HAYNES 230 alloy: Typical room temperature LT stress-strain curve for 0.50–0.75-inch-thick plate

3.2.1.2 *[Table]* HAYNES 230 alloy: Average room temperature tensile properties for solution-annealed sheet and plate

3.2.1.3 *[Figure]* HAYNES 230 alloy: Variation of room temperature ultimate tensile strength with exposure time at 1200F, 1400F and 1600F

3.2.1.4 *[Figure]* HAYNES 230 alloy: Variation of room temperature 0.2% yield strength with exposure time at 1200F, 1400F, and 1600F

The long-time exposure of HAYNES 230 alloy in the 1200F–1600F temperature range results in an increase of 4–7% in the ultimate tensile strength. The 0.2% yield strength increased about 12% after long-time exposures at 1200F. For exposures at 1400F, the yield strength decreased initially, then increased to about 6% above the baseline after 16,000 hours. Exposures at 1600F resulted in a slight decrease in the yield strength, and then it increased to about equivalent to the baseline value after 16,000 hours. The tensile elongations exhibited a rapid decrease with time for all the exposure temperatures, and then the values tended to plateau in the 33–37% range for longer exposure times. The decline in ductility was related to the precipitation of $M_{23}C_6$ carbides. The fracture surfaces of the broken tensile specimens indicated predominantly ductile fracture. (Refs. 2, 27, 28)

3.2.1.5 *[Figure]* HAYNES 230 alloy: Variation of room temperature tensile elongation with exposure time at 1200F, 1400F, and 1600F

HAYNES 230 alloy undergoes long range ordering when aged in the 842–1022F (450–550C) temperature range. This results in increases in the yield strength and ductility properties of the alloy. (Ref. 10)

3.2.1.6 *[Table]* HAYNES 230 alloy: Relative change in room temperature tensile properties for samples aged for various times at 932F (500C) and 1022F (550C)

3.2.2 Compression Stress-Strain Diagrams and Compression Properties

3.2.2.1 *[Figure]* HAYNES 230 alloy: Room temperature compression stress-strain curves at strain rates of 0.001/s and 3000/s

3.2.3 Impact

3.2.3.1 *[Figure]* HAYNES 230 alloy: Room temperature Charpy-V impact strength after exposures to 1200F, 1400F and 1600F

The thermal stability of HAYNES 230 alloy is superior to several solid-solution-strengthened alloys. This is attributed to the fact that the alloy only has precipitates of $M_{23}C_6$ carbides following long-term exposures in the 1200F–1600F temperature range. (Refs. 27, 28)

3.2.3.2 *[Table]* Comparative room temperature Charpy-V impact strengths following 8,000 hour exposures at temperatures of 1200F, 1400F and 1600F for several nickel-base alloys

The long-range ordering reaction that was observed to occur in the 932–1022F (500-550C) temperature resulted in an increase in Charpy-V toughness.

3.2.3.3 *[Table]* HAYNES 230 alloy: Average Charpy-V impact strength after aging at 932F (500C) and 1022F (550C) for 1000 hours

3.2.4 Bending

3.2.5 Torsion and Shear

3.2.6 Bearing

3.2.7 Stress Concentration

3.2.7.1 Notch Properties

3.2.7.2 Fracture Toughness

3.2.7.2.1 *[Table]* HAYNES 230 alloy: Average room temperature fracture toughness data for 1-inch-thick plate

3.3 Mechanical Properties at Various Temperatures

3.3.1 Tension Stress-Strain Diagrams and Tensile Properties

3.3.1.1 *[Table]* HAYNES 230 alloy: Average tensile properties from 77 to -452F for 0.025–0.040-inch-thick sheet

3.3.1.2 *[Figure]* HAYNES 230 alloy: Typical room temperature-300F, LT stress-strain curves for 0.50–0.75-inch-thick plate

3.3.1.3 *[Figure]* HAYNES 230 alloy: Typical stress-strain curves from 400–800F for 0.50–0.75-inch-thick plate, LT

3.3.1.4 *[Figure]* HAYNES 230 alloy: Typical stress-strain curves from 1000–1400F for 0.50–0.75-inch-thick plate, LT

3.3.1.5 *[Figure]* HAYNES 230 alloy: Typical stress-strain curves from 1600–1800F for 0.50–0.75-inch-thick plate, LT.

3.3.1.6 *[Figure]* HAYNES 230 alloy: Tensile properties for sheet from room temperature to 2000F

3.3.1.7 *[Figure]* HAYNES 230 alloy: Tensile properties for plate from room temperature to 2000F

3.3.2 Compression Stress-Strain Diagrams and Compression Properties

A great deal of compression stress-strain data has been generated for HAYNES 230 alloy at elevated temperatures in order to define its high temperature deformation characteristics. The data ranges from temperatures of 1741–2191F and strain rates of 0.1–20/s. Figure 3.3.2.1 shows some of this data for a strain rate of 0.1/s. (Ref. 30)

3.3.2.1 *[Figure]* HAYNES 230 alloy: Compression stress-strain curves from 1741–2011F at a strain rate of 0.1/s

3.3.3 Impact

3.3.4 Bending

3.3.5 Torsion and Shear

3.3.6 Bearing

3.3.7 Stress Concentration

3.3.7.1 Notch Properties

3.3.7.2 Fracture Toughness

3.3.8 Combined Loading

3.4 Creep and Rupture Properties

Like similar solid-solution-strengthened alloys, the creep strength of HAYNES 230 alloy can be affected by secondary thermomechanical processing. The following tables illustrate the effects of strain plus subsequent heat treatment and the effects of secondary heat treatments alone on the low strain creep strength of the alloy. (Ref. 32)

3.4.1 *[Table]* HAYNES 230 alloy: Creep and rupture properties of solution-annealed sheet

3.4.2 *[Table]* HAYNES 230 alloy: Creep and rupture properties of solution-annealed bar and plate

Exposing HAYNES 230 alloy to intermediate high temperatures such as 1400F (760C) and 1600F (871C) results in significant $M_{23}C_6$ carbide precipitation. This results in increased stress-rupture life which is believed to be due to a decrease in the rate of grain boundary sliding during creep. If the alloy is given a

rejuvenation heat treatment, the stress-rupture properties are as good as or slightly higher than the original properties as illustrated in the following tables. (Ref. 33)

3.4.3 *[Table]* Effects of thermomechanical cycles on 1600F (870C)/7 ksi (48 MPa) creep properties for several nickel-base alloys

3.4.4 *[Table]* Effects of secondary heat treatments on 1600F (870C)/7 ksi (48 MPa) creep properties for several nickel-base alloys

3.4.5 *[Table]* HAYNES 230 alloy: Average 1700F (927C)/9 ksi (62 MPa) stress-rupture data for 230 alloy plate for the as-received, exposed and rejuvenated conditions

3.5 Fatigue Properties

3.5.1 High-Cycle Fatigue (HCF)

3.5.1.1 *[Figure]* HAYNES 230 alloy: High-cycle fatigue behavior of 0.75-inch-thick plate at 1400F

3.5.1.2 *[Figure]* HAYNES 230 alloy: High-cycle fatigue behavior of 0.75-inch-thick plate at 1800F

3.5.2 Low-Cycle Fatigue (LCF)

Exposure to intermediate temperatures such as 1400F can exert a toll on LCF lives at temperatures below about 1200F because debits in ductility produced by the exposures remain unrelieved. The fatigue lives of HAYNES 230 alloy are least affected because only $M_{23}C_6$ carbides precipitate during such an exposure. In the case of X and 188 alloys, intermetallic compounds such as sigma and Laves phases precipitate in addition to the carbides. These phases significantly reduce low temperature ductility. This is illustrated in the following tables. (Ref. 37)

3.5.2.1 *[Figure]* HAYNES 230 alloy: Low-cycle fatigue properties for 0.625-ich-thick plate at elevated temperatures

3.5.2.2 *[Figure]* HAYNES 230 alloy: Low-cycle fatigue behavior of 0.125-inch-thick sheet at elevated temperatures

It is well understood that grain size has a very important effect on the low-cycle fatigue resistance of a material. This is illustrated for HAYNES 230 alloy in the following figures in which the fatigue lives of bar processed at temperatures of 2050F (1121C) and 2250F (1232C) exhibit differing behavior. The grain sizes for the two conditions were ASTM 8 (~ 20 µm) and ASTM 5 (~ 70 µm) respectively. The fatigue lives of the finer grain size material was about twice that of the standard grain size material for the tests performed at 1800F. (Ref. 38)

3.5.2.3 *[Table]* Effect of aging at 1400F/1000 hours on the 800F low-cycle fatigue lives of several solid-solution-strengthened superalloys (plate and bar samples, R = -1, f = 0.33 Hz)

3.5.2.4 *[Figure]* HAYNES 230 alloy: Effect of processing temperature on the 1400F low-cycle fatigue behavior of 0.75-inch-diameter bar

3.5.2.5 *[Figure]* HAYNES 230 alloy: Effect of processing temperature on the 1600F low-cycle fatigue behavior of 0.75-inch-diameter bar

3.5.2.6 *[Figure]* HAYNES 230 alloy: Effect of processing temperature on the 1800F low-cycle fatigue behavior of 0.75-inch-diameter bar

Tensile holds can have very damaging effects on the low-cycle fatigue lives of a material. This is shown in the following figure. (Ref. 39)

3.5.2.7 *[Figure]* HAYNES 230 alloy: Effect of tensile hold times on the fatigue lives of 0.125-inch-thick sheet at a total strain range of 1.0%

3.5.3 Fatigue Crack Growth

For tests performed at 1500F with no tensile hold, the fatigue crack propagation occurred in a transgranular mode with well-defined fatigue striations. Imposing a 2-minute hold resulted in a predominantly intergranular fracture mode. For tests performed at 1700F with no tensile hold, fatigue crack propagation was predominantly intergranular. The imposition of a 2-minute tensile hold resulted in a completely intergranular fracture mode. (Ref. 40)

3.5.3.1 *[Figure]* HAYNES 230 alloy: Fatigue crack growth with and without 2-minute tensile holds at 1500F and 1700F

3.6 Elastic Properties

3.6.1 Poisson's Ratio

3.6.1.1 *[Figure]* HAYNES 230 alloy: Effect of temperature on Poisson's ratio

3.6.2 Modulus of Elasticity

3.6.2.1 *[Figure]* HAYNES 230 alloy: Effect of temperature on the dynamic modulus of elasticity

3.6.3 Modulus of Rigidity

3.6.4 Tangent Modulus

3.6.5 Secant Modulus

4.0 Fabrication

4.1 Forming

HAYNES 230 alloy has good forming characteristics. The recommended temperature range for hot working is 1800–2200F. Hot working practices which incorporate heavy initial and moderate final reductions along with frequent reheating usually provide the best results. The alloy can be readily formed into various configurations by cold forming. The alloy tends to work harden more rapidly than a stainless steel, thereby requiring a greater amount of force for the

same reduction. Furthermore, more frequent intermediate annealing between forming steps may be required to make a finished part. Solution annealing is carried out in the 2125–2250F temperature range for a time that is commensurate with the part thickness. (Ref. 6)

4.2 Machining and Grinding

The machining characteristics of HAYNES 230 alloy are similar to solid-solution-strengthened nickel-base alloys. Since these alloys tend to work harden more rapidly than stainless steels, it is recommended to use slower feeds and heavier cuts. The alloy can be machined using conventional methods at satisfactory rates. (Refs. 2, 6)

4.3 Joining

HAYNES 230 alloy is readily welded by gas tungsten arc (GTAW), gas metal arc (GMAW), shielded metal arc (SMAW), and resistance welding techniques. Its welding characteristics are similar to those for HASTELLOY X alloy. Submerged arc welding is not recommended due to factors that can increase weld hot cracking. HAYNES 230-W filler metal (AMS 5839) is recommended for joining 230 alloy by GTAW or GMAW. Coated electrodes of 230-W alloy are available for SMAW. For the dissimilar welding of 230 alloy to nickel-, iron- or cobalt-base alloys, 230-W filler wire, HAYNES 556 (AMS 5831), HASTELLOY S alloy (AMS 5838) or HASTELLOY W alloy (AMS 5786, AMS 5787) welding products can be used depending on the particular case. (Refs. 2, 6) As shown in Table 4.3.1, GMAW deposits of 230-W filler metal have lower ultimate tensile strengths, higher yield strengths and comparable ductilities in comparison to typical plate products. Weldments have good tensile properties, as shown in Table 4.3.2. Weldments that were exposed to 1600F/1500 hours had slightly higher ultimate tensile strengths, similar yield strengths and slightly lower ductilities than the weldments in the as-received condition. When the weldments were given a rejuvenation heat treatment, the ultimate tensile strengths were slightly higher than the as-received condition, but the yield strengths and ductilities were comparable. All of the weldments passed root and face bend tests with no evidence of weld defects. (Refs. 2, 33)

4.3.1 *[Table]* Tensile properties for GMAW deposits of HAYNES 230-W weld metal

4.3.2 *[Table]* Room temperature tensile data for HAYNES 230 alloy plate GTAW weldments made using 230-W filler metal

4.4 Surface Treating

Due to its composition, HAYNES 230 alloy develops a very adherent oxide scale when exposed to elevated temperatures. Removal of such scales is best done by immersing the alloy in a molten caustic bath followed by acid pickling. (Ref. 6)

References

1. D. L. Klarstrom, "The Development of HAYNES 230 Alloy," *Materials Design Approaches and Experiences*, J. C. Zhao, et al. editors, TMS, Warrendale, PA, 2001, pp. 297–307.
2. "HAYNES 230 Alloy," Brochure 3000H, Haynes International, Inc., 2004.
3. "Applicable Specifications," Brochure H-1034M, Haynes International, Inc., 2004.
4. AMS 5878C, Society of Automotive Engineers, 2007.
5. AMS 5891B, Society of Automotive Engineers, 2007.
6. "Fabrication of HAYNES and HASTELLOY Solid-Solution Strengthened High Temperature Alloys," Brochure 3159A, Haynes International, Inc., 2002.
7. D. Ulmer, "Hydrogen Embrittlement of HAYNES 230," 5th NASA/NASP Workshop on Hydrogen-Materials Interactions, 1992.
8. D. L. Klarstrom, et al., "A New Gas Turbine Combustor Alloy," ASME Paper 84-GT-70, Intl. Gas Turbine Conf., Holland, June 3–7, 1984.
9. L. M. Pike and S. K. Srivastava, "Long Term Thermal Stability of Several Gas Turbine Alloys," ASME Paper GT2005-68959, ASME Turbo Expo 2005, June 6–9, 2005, Reno-Tahoe, Nevada.
10. Å. Martinsson, "Ageing Influence on Nickel-based Superalloys at Intermediate Temperatures (400–600°C)," M.S. Thesis, Luleå University of Technology, Sweden, 2006.
11. J. R. Markham, et al., "Bench top Fourier transform infrared based instrument for simultaneously measuring surface spectral emittance and temperature," *Rev. Sci. Instrum.*, 64(9), September 1993, pp. 2515–22.
12. B. V. Cockeram, et al., "The development of emissivity enhancement coatings for thermophotovoltaic (TPV) radiator applications," *Thin Solid Films*, Vols. 355–56, Nov. 1, 1999, pp. 17-25.
13. "HASTELLOY X alloy," Brochure H-3009A, Haynes International, Inc., 1997.
14. J. R. Dillman, Unpublished data, Haynes International, Inc., 1988.
15. M. A. Harper, et al., "Long-Term Oxidation Behavior of Selected High Temperature Alloys," Paper No. 132, Corrosion 97, NACE, Houston, TX, 1997.
16. V. P. Deodeshmukh and S. K. Srivastava, "Long–Term Cyclic Behavior of Selected High Temperature Alloys," *Superalloys 2008*, TMS, Warrendale, PA, 2008.
17. D. M. England and A. V. Vikar, "Oxidation Kinetics of Some Nickel-Based Superalloy Foils in Humidified Hydrogen and Electronic Resistance of the Oxide Scale Formed," *J. Electrochemical Soc.*, 148(4) A330-A338, 2001.
18. G. Y. Lai, et al., "A Burner Rig Investigation of the Hot Corrosion behavior of Several Wrought Superalloys and Intermetallics," ASME Paper 91-GT-21, International Gas Turbine and Aeroengine Congress and Exposition, Orlando, FL, 1991.
19. J. J. Barnes and G. Y. Lai, "Factors Affecting The Nitridation Behavior of Fe-base, Ni-base and Co-base Alloys in Pure Nitrogen," *Proc. 3rd Intl. Symp. On High Temperature Alloys*, Les Embiez, France, 1992.
20. G. Y. Lai, "Nitridation Attack in a Simulated Gas Turbine Combustion Environment," *Materials for Advanced Power Engineering, Part II*, Kluwer Academic Publishers, The Netherlands, 1994, pp. 1263–71.
21. D. L. Klarstrom and H. J. Grabke, "The Metal Dusting Behavior of Several High emperature Nickel Based Alloys," NACE Paper 1379, Corrosion 2001, Houston, TX, 2001.
22. K. Natesan and Z. Zeng, "Development of Materials Resistant to Metal Dusting Degradation," Final Report ANL-07/30, Oct., 2007.
23. AMS Specifications 5878C and 5891B, SAE International, Warrendale, PA, 2007.
24. ASTM Specifications B 435, B 564, B 572, B 619, B 622, B 626, ASTM International, West Conshocken, PA, 2007.
25. D. L. Klarstrom, Haynes International, Inc., unpublished data.
26. Metallic Materials Properties Development and Standardization (MMPDS-02), Battelle Memorial Laboratories, Columbus, OH, 2005.
27. D. L. Klarstrom, "The Thermal Stability of a Ni-Cr-W-Mo Alloy," Paper 407, Corrosion 94, NACE, Houston, TX, 1994.
28. L. M. Pike and S. K. Srivastava, "Long Term Thermal Stability of Several Gas Turbine Alloys," Paper GT2005-68959, ASME Turbo Expo 2005, Reno-Tahoe, NV, 2005.
29. K. Vecchio and G. T. Gray, "Effects of Shock Loading on a Solid-Solution Strengthened Superalloy," *Proc. of the Joint AIRAPT/APS Conf.*, June, 1993, American Physical Soc., 1994, pp. 1213–16.
30. P. Chaudhury and D. Zhao, "Atlas of Formability: Haynes 230," National Center for Excellence in Metalworking, Johnstown, PA, 1992.

31. R. R. Seeley and S. K. Srivastava, "The Effect of Long-Term Thermal Exposure on the Mechanical Properties of Four Modern High-Temperature Nickel-Base Alloys," *Long Term Stability of High-Temperature Materials*, G. E. Fuchs, K. A. Dannemann and T. C. Deragon, Eds., TMS, 1999.

32. D. L. Klarstrom, H. M. Tawancy and M. F. Rothman, "Structure/Property Relationships in Solid-Solution Strengthened Superalloys," *Superalloys 1984, Proc. 5th Intl. Symposium on Superalloys*, Seven Springs, PA, Oct. 7–11, 1984, pp. 553–62.

33. D. L. Klarstrom, et al., "Rejuvenation Heat Treatment and Weld Repairability Studies of HAYNES 230 Alloy," ASME Paper No. 2000-GT-629, Intl. Gas Turbine and Aeroengine Congress, Munich, Germany, May 8–11, 2000.

34. R. R. Seeley, et al., "Fatigue in Modern Nickel-Base Alloys for Gas Turbine Applications," *Life Assessment of Hot section Gas turbine Components*, Cambridge University Press, UK, 2000, pp. 61–82.

35. S. K. Srivastava and D. L. Klarstrom, "The LCF Behavior of Several Solid Solution Strengthened Alloys Used in Gas Turbine Engines," ASME Paper 90-GT-80, Intl. Gas Turbine Conf., Brussels, Belgium, June 11–14, 1990.

36. R. L. McDaniels, et al., "A Comparative Study of the Low-Cycle Fatigue Behavior of Several Superalloys," *Maintenance and Reliability Conf.*, Gatlinburg, TN, May 6–9, 2001.

37. D. L. Klarstrom and G. Y. Lai, "Effects of Aging on the LCF Behavior of Three Solid-Solution Strengthened Superalloys," *Superalloys 1988, Proc. 6th Int. Symposium on Superalloys*, Seven Springs, PA, Sept. 18–22, 1988, pp. 585–94.

38. K. S. Vecchio, M. D. Fitzpatrick and D. L. Klarstrom, "Influence of Subsolvus Processing on the Low Cycle Fatigue Properties of HAYNES 230 alloy," *Met. & Matls. Trans. A*, 26A, 1995, pp. 673–89.

39. L. J. Chen, et al., "High Temperature Low-Cycle Fatigue Behavior of HAYNES 230 Superalloy," *Superalloys 2000*, TMS, Seven Springs, PA, Sept. 17–21, 2000, pp. 573–81.

40. S. Y. Lee, et al., "Elevated-Temperature Creep-Fatigue Crack Growth Behavior of Nickel-Based HAYNES R-41, 230, and HASTELLOY X alloys," *Superalloys 2008*, TMS, 2008, pp. 509–14.

41. M. Katcher, Unpublished Data, Haynes International, 2006.

Table 1.3.1 HAYNES 230 Alloy: AMS and ASTM specifications (Refs. 2, 3)

Specification	Product Forms
AMS	
5878	Sheet, plate and strip
5891	Bars, forgings and rings
ASTM	
B 435	Sheet and plate
B 572	Rod
B 619	Welded pipe
B 622	Seamless pipe and tube
B 564	Forgings
B 472	Billets and bars for reforging

Table 1.4.1 HAYNES 230 alloy: AMS specification limits

Element	Alloy Content (weight percent)	
	Minimum	Maximum
Carbon	0.05	0.15
Manganese	0.3	1
Silicon	0.25	0.75
Phosphorus	--	0.03
Sulfur	--	0.015
Chromium	20	24
Molybdenum	1	3
Tungsten	13	15
Aluminum	0.2	0.5
Lanthanum	0.005	0.05
Cobalt	--	5
Titanium	--	0.1
Boron	--	0.015
Iron	--	3
Copper	--	0.5
Nickel	remainder	

Table 1.6.1 HAYNES 230 Alloy: Hardness of various product forms

Product Form	Hardness (R_B)	Pieces Tested
Sheet	92.5	37
Plate	95.2	26
Bar	92.7	24

Table 1.6.2 HAYNES 230 Alloy: Hardness after imposed coldwork (Ref. 6)

Alloy: HAYNES 230 **Hardness for indicated % coldwork**					
0	10	20	30	40	50
95 R_B	28 R_C	35 R_C	39 R_C	40 R_C	42 R_C

Table 1.9.1 HAYNES 230 Alloy: Hydrogen embrittlement resistance

Alloy: HAYNES 230		
Temperature (F)	**H_2 Pressure (psig)**	**Ratio of Notched Tensile Strength (H_2/Air)**
70	3000	0.92
70	5000	1.07
1200	3000	1
1600	3000	1

Tests were performed in MIL-P-27201B grade hydrogen with a crosshead speed of 0.005 in/min. Specimens were notched with a K_t value of 8.0 (Ref. 2)

Table 2.1.2.1 HAYNES 230 Alloy: Maximum shrinkage after 3000 hour exposures in the 842-1022F (450-550C) temperature range (Ref. 10)

Exposure Temperature (F)	Exposure Temperature (C)	Maximum Shrinkage (%)
842	450	0.04
932	500	0.052
1022	550	0.046

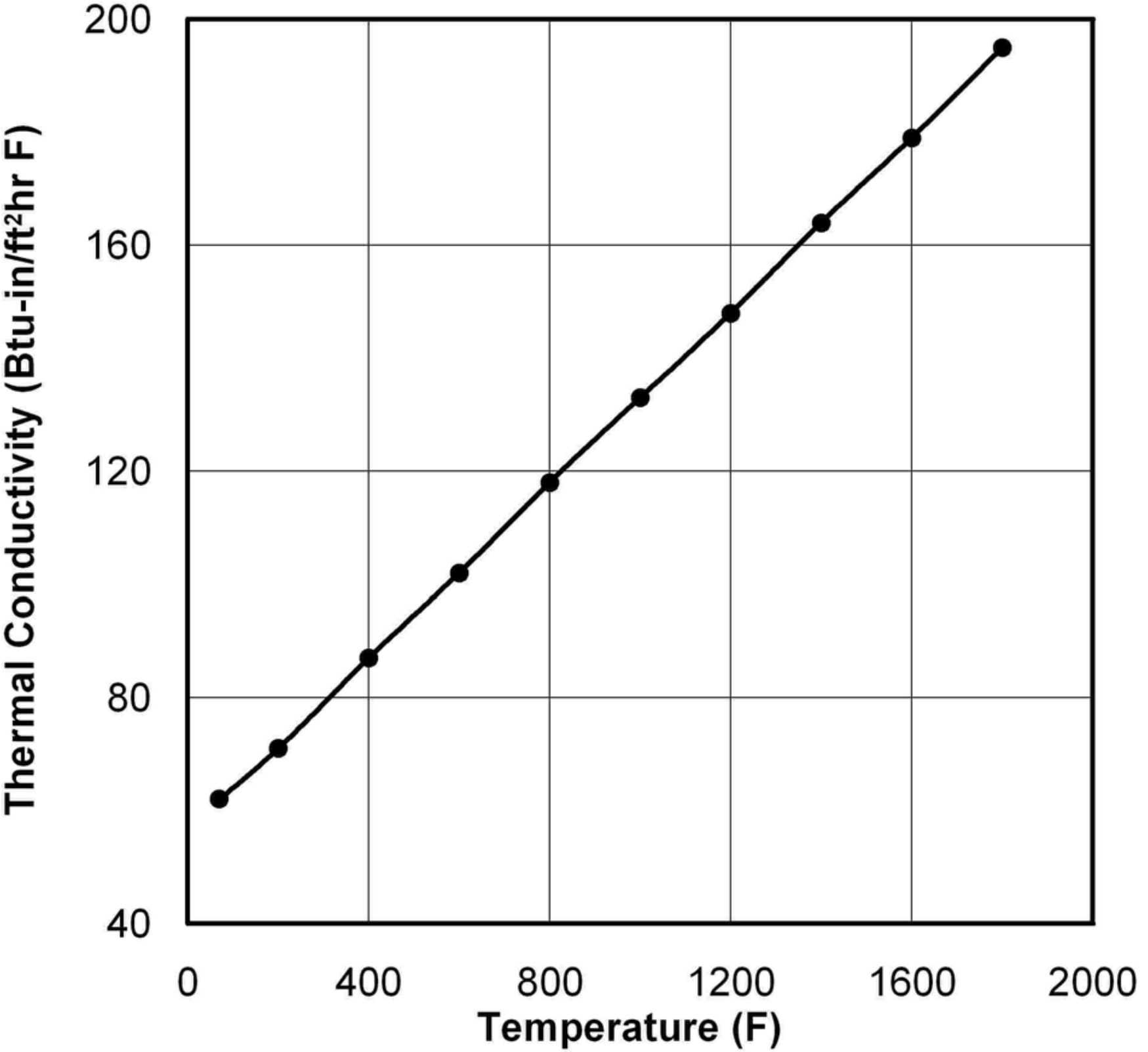

Figure 2.1.3.1 HAYNES 230 alloy: Thermal conductivity (Ref. 2)

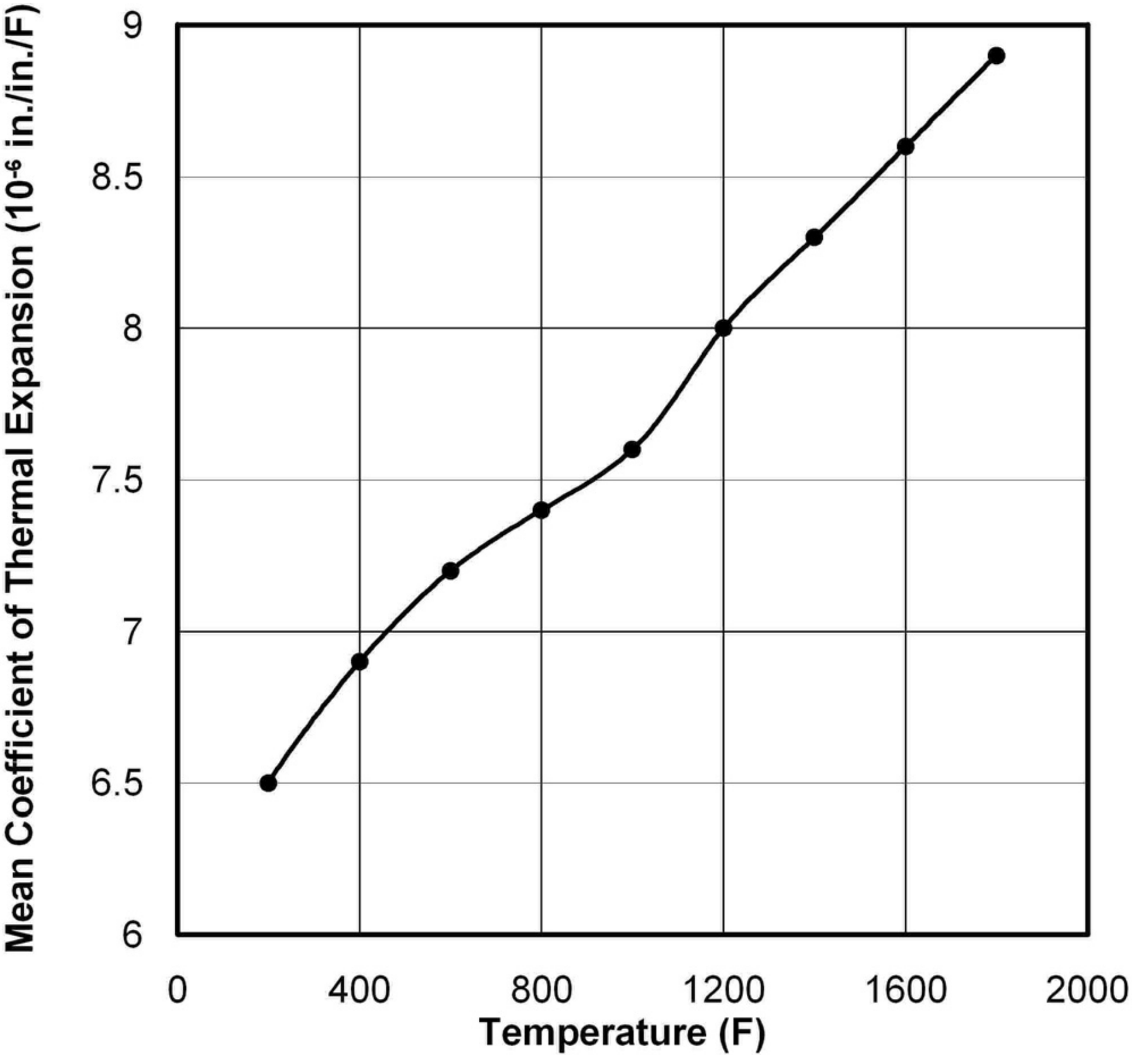

Figure 2.1.4.1 HAYNES 230 alloy: Mean coefficient of thermal expansion (Ref. 2)

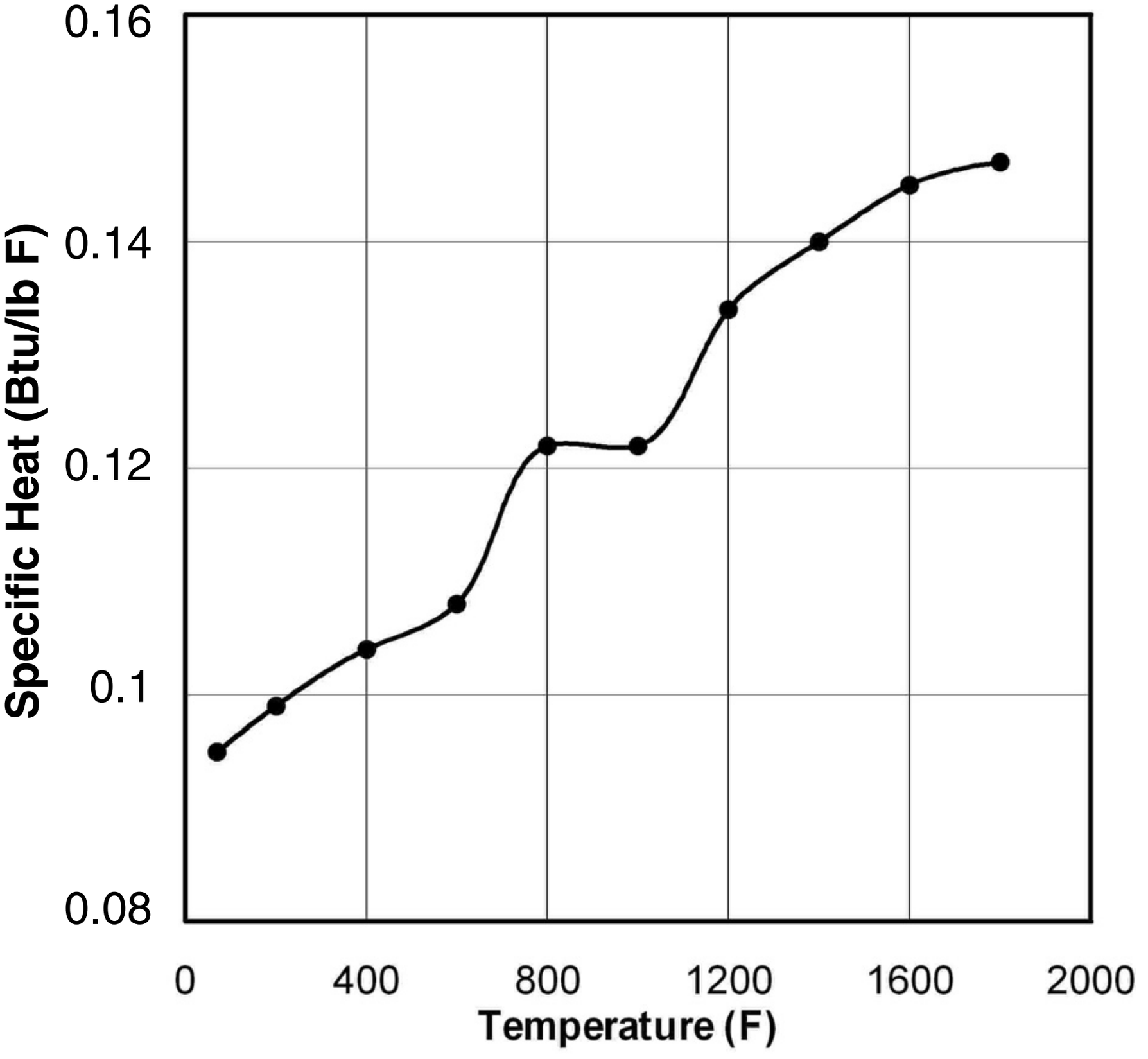

Figure 2.1.5.1 HAYNES 230 alloy: Specific heat (Ref. 2)

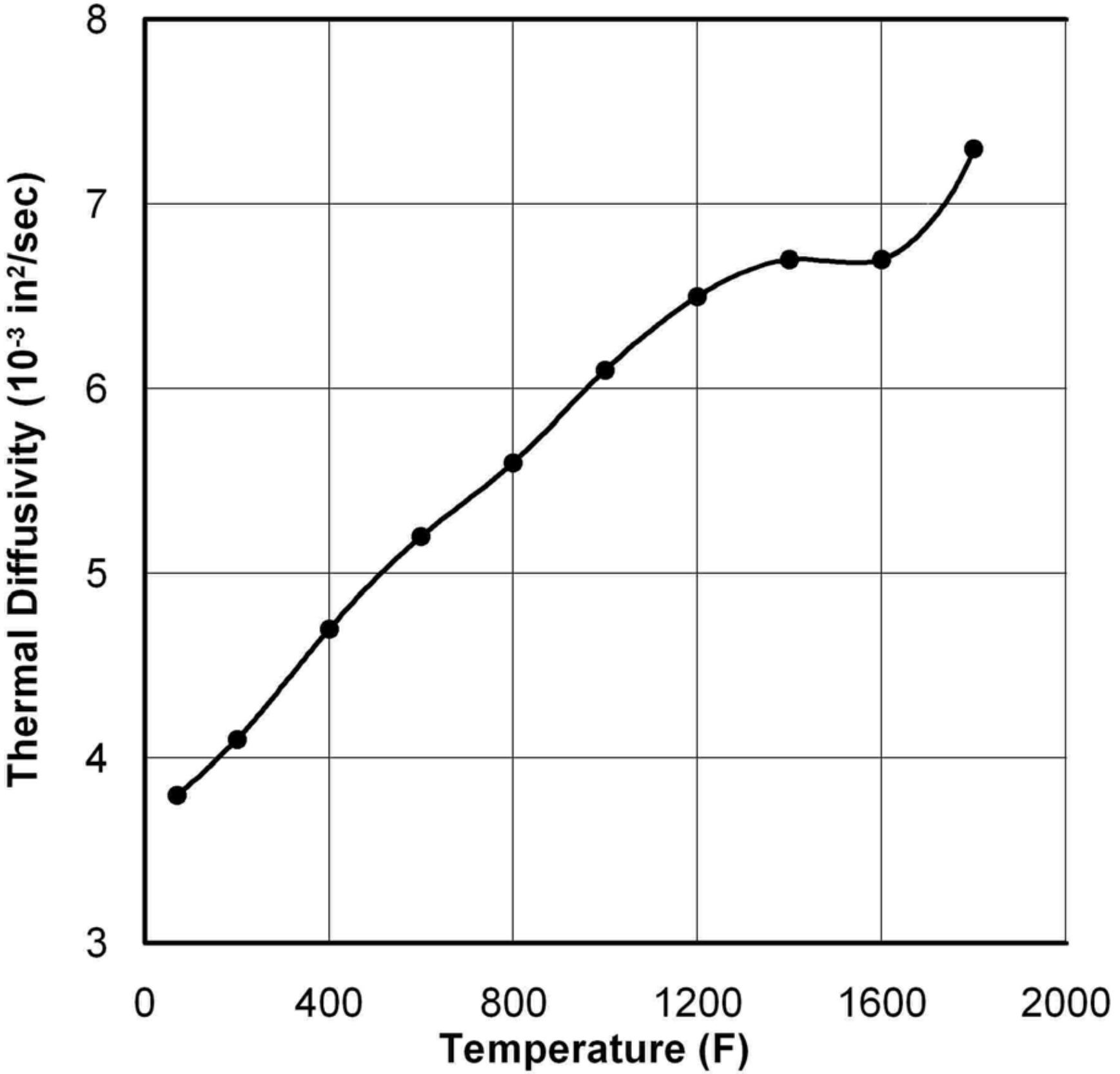

Figure 2.1.6.1 HAYNES 230 alloy: Thermal diffusivity (Ref. 2)

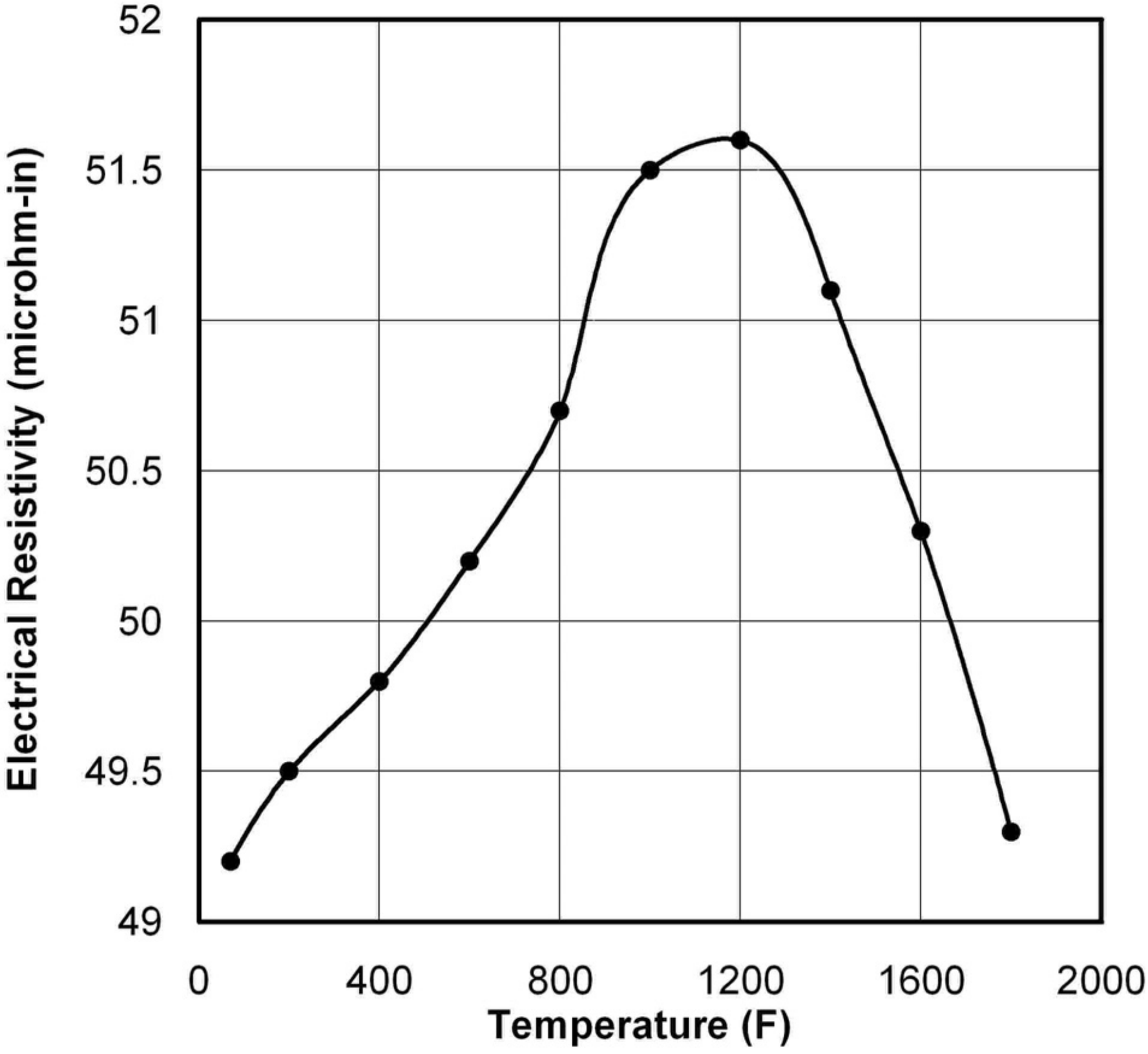

Figure 2.2.2.1 HAYNES 230 alloy: Electrical resistivity (Ref. 2)

Table 2.3.1.1 Aqueous corrosion resistance for several nickel-base alloys (Ref. 2)

Alloy	Corrosion Rate (mils/yr)		
	10% HNO_3 Boiling	10% H_2SO_4 150F (66C)	10% HCl 150F (66C)
230	0.3	0.6	112
625	0.7	0.4	65
600	0.8	41.8	366
316 SS	1	17.8	3408
X	-	<0.1	99

Table 2.3.3.1 Short-term oxidation in flowing air for several nickel-base alloys. Test was conducted for 1008 hours with an air flow rate of 7.0 ft/min (213.4 cm/min) past the samples. (Ref. 2)

	Average Metal Affected							
	1800F (982C)		2000F (1093C)		2100F (1149C)		2200F (1204C)	
Alloy	(Mils)	(µm)	(Mils)	(µm)	(Mils)	(µm)	(Mils)	(µm)
230	0.7	18	1.3	33	3.4	86	7.9	201
188	0.6	15	1.3	33	8	203	>21.7	>551
601	1.3	33	2.6	66	5.3	135	7.5*	191*
X	0.9	23	2.7	69	5.8	147	>35.4	>889
625	0.7	18	4.8	122	18.2	462	>47.6	>1209
800H	1.8	46	7.4	188	8.9	226	13.6	289
446SS	2.3	58	14.5	368	>21.7	>551	>23.3	>592
316SS	14.3	363	>68.4	>1737	>105	>2667	>140.4	>3566

*601 sample exhibited very large internal voids.

Table 2.3.3.2 Long-term oxidation resistance in still air for several nickel-base alloys. Samples were cycled to room temperature every 30 days. (Ref. 15)

Alloy	Average Metal Affected					
	1800F (982C)/ 720 days		2000F (1093C)/ 360 days		2100F (1149C)/ 360 days	
	(Mils)	(µm)	(Mils)	(µm)	(Mils)	(µm)
230	5.8	147	10.7	272	34	864
617	9.4	239	-	-	37.2	945
HR-120	12.2	310	2.6	66	53	1346
556	15.2	386	21.2	538	-	-
HR-160	16.7	424	29	737	58.7	1491
601	22.4	569	45.1	1146	72.8	1849
RA85H	53.7	1364	80.3	2040	94.8	2408
800HT	79.8	2027	51	1295	70.3	1786

Table 2.3.3.3 Long-term oxidation resistance in flowing air for several nickel-base alloys. Samples were cycled to room temperature every 30 days. (Ref. 16)

Alloy	Average Metal Affected					
	1800F (982C)/ 360 days		2000F (1093C)/ 360 days		2100F (1149C)/ 360 days	
	(Mils)	(µm)	(Mils)	(µm)	(Mils)	(µm)
230	2.5	64	11	279	34.4	874
X	2.8	71	26.2	665	55.4	1407
HR-120	3.3	84	23.2	589	44	1118
556	6.2	157	34.1	866	-	-
HR-160	13.7	348	30.7	780	45.6	1158

Table 2.3.3.4 Burner rig oxidation resistance at 1800F (982C) for 1000 hours for several nickel-base alloys. Samples were cycled to near ambient temperature every 30 minutes. (Ref. 2)

	Metal Loss		Average Metal Affected		Maximum Metal Affected	
Alloy	(Mils)	(µm)	(Mils)	(µm)	(Mils)	(µm)
230	0.8	20	2.8	71	3.5	89
188	1.1	28	3.5	89	4.2	107
X	2.7	69	5.6	142	6.4	163
625	4.9	124	7.1	180	7.6	193
330	7.8	198	10.6	269	11.8	300
310SS	13.7	348	16.2	406	16.5	419
600	12.3	312	14.4	366	17.8	452
601	3	76	18.8	478	20	508

Table 2.3.4.1 Hot corrosion resistance at 1650F (900C) for several nickel-base alloys. Artificial sea salt was injected into the combustion gases at the levels indicated. The tests were cycled to less than 400F every hour. (Ref. 18)

Alloy	Average Metal Affected					
	5 ppm Salt		50 ppm Salt			
	1000 hrs		200 hrs		1000 hrs	
	(Mils)	(µm)	(Mils)	(µm)	(Mils)	(µm)
188	2.8	71	1.6	41	3.2	81
230	5.1	130	2.4	61	4.4	112
X	5.5	140	2.8	71	>46.0	>1168
25	>43	>1092	2.8	71	>37.8	>960

Table 2.3.5.1 Nitrogen absorption in flowing NH_3 after 168 hours for several nickel-base alloys (Ref. 2)

Alloy	Nitrogen Absorption (mg/cm^2)	
	1200F (650C)	1800F (982C)
230	0.7	1.4
600	0.8	0.9
625	0.8	2.5
X	1.7	3.2
330	3.9	-
800H	4.3	4
316SS	6.9	6
310SS	7.4	7.7
304SS	9.7	7.3

Table 2.3.5.2 Nitrogen absorption and internal penetration in N_2 at 2000F (1093C) for 168 hours for several nickel-base alloys (Ref. 19)

Alloy	Nitrogen Absorbed (mg/cm^2)	Average Internal Penetration (mm)
600	1.1	0.41
230	2.7	0.46
188	3.7	>0.51
617	5.1	>0.58
X	6	0.63
330	6.6	>1.52
601	7.2	>0.59
556	9	>1.52
800H	10.3	>1.46

Table 2.3.5.3 Nitrogen pick-up following burner rig testing at 1800F (980C) for 1000 hours with 30-minute cycling for several nickel-base alloys (Ref. 20)

Alloy	Nitrogen Content (wt %)	
	Original	After Testing
230	0.05	0.06
263	0.004	0.42
617	0.03	0.52
X	0.04	0.57

Table 2.3.6.1 Final metal wastage rates in a gas with a carbon activity of 18.9 at 1200F (650C) and 1 atm pressure for several nickel-base alloys (Ref. 21)

Alloy	Total Exposure Time (hrs)	Final Metal Wastage Rate (mg/cm^2h)
HR-120	190	4.1×10^{-2}
800H	925	2.7×10^{-3}
214	5,707	1.0×10^{-3}
601	10,000	2.5×10^{-3}
230	10,000	3.2×10^{-4}
HR-160	10,000	0.0*

*Attack too small for analysis

Table 3.1.1.1 HAYNES 230 Alloy: Room temperature tensile requirements for AMS and ASTM specifications (Refs. 23, 24)

Specification	Minimum Room Temperature Tensile Properties		
	Tensile Strength (ksi)	0.2% Yield Strength (ksi)	Elongation in 2 in. (%)
AMS 5878C	115	50	40
AMS 5891B	110	45	35
ASTM*	110	45	40

*B 435, B 564, B 572, B 619, B 622, B 626

Table 3.1.1.2 HAYNES 230 Alloy: Stress rupture requirements for AMS specifications (Ref. 23)

Specification	Temperature (F)	Stress (ksi)	Minimum Life (hrs)	Minimum Elongation (%)
AMS 5878C	1700	9	36	10
AMS 5891B	1700	9	24	10

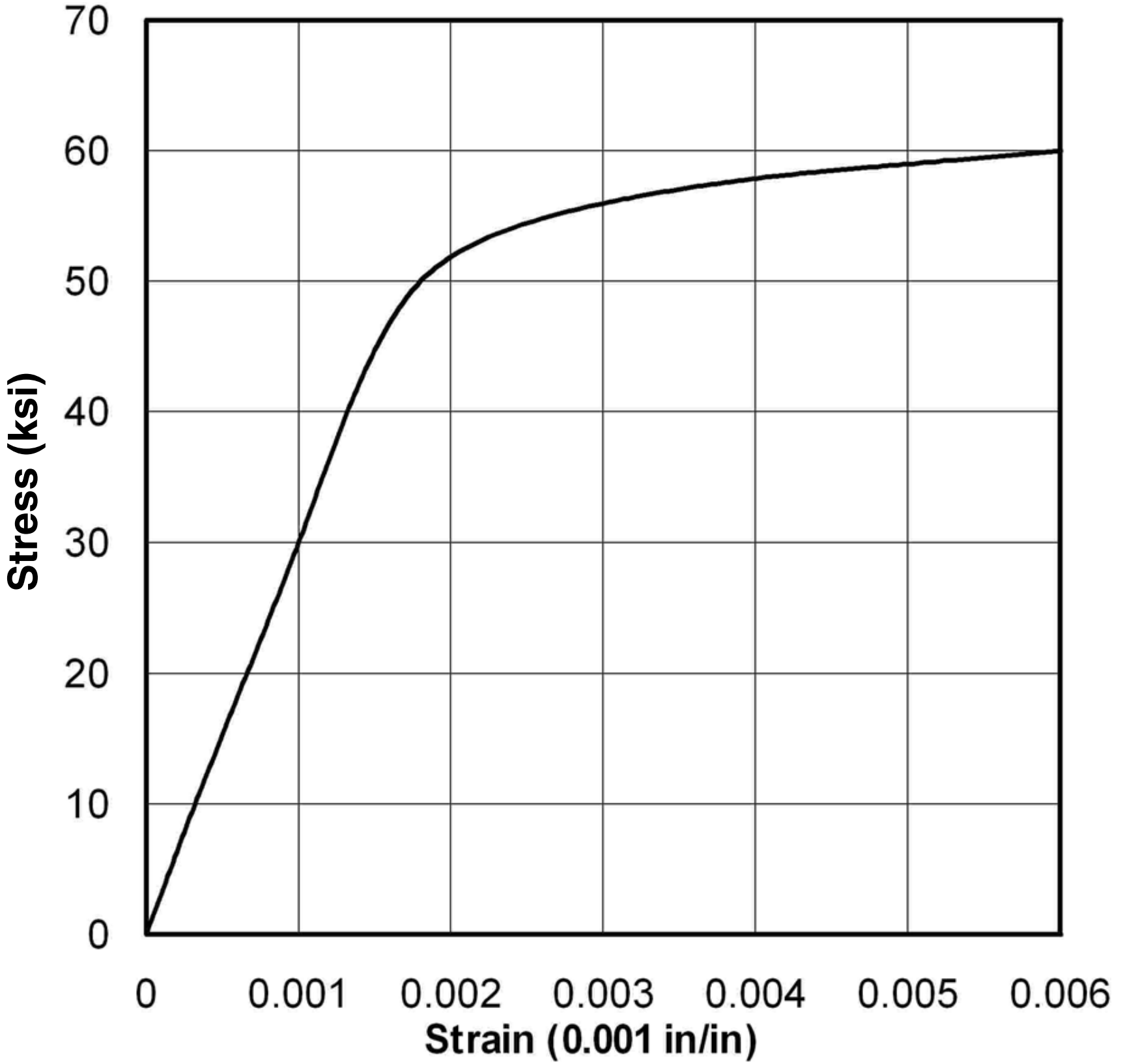

Figure 3.2.1.1 HAYNES 230 alloy: Typical room temperature LT stress-strain curve for 0.50–0.75-inch-thick plate (Ref. 26)

Table 3.2.1.2 HAYNES 230 Alloy: Average room temperature tensile properties for solution-annealed sheet and plate (Ref. 2)

Form	Orientation	F_{ty} (ksi)	F_{tu} (ksi)	Elongation in 2 in. (%)
Sheet	T	61.3	121.6	47.2
Plate	T	54.4	121.8	47.7

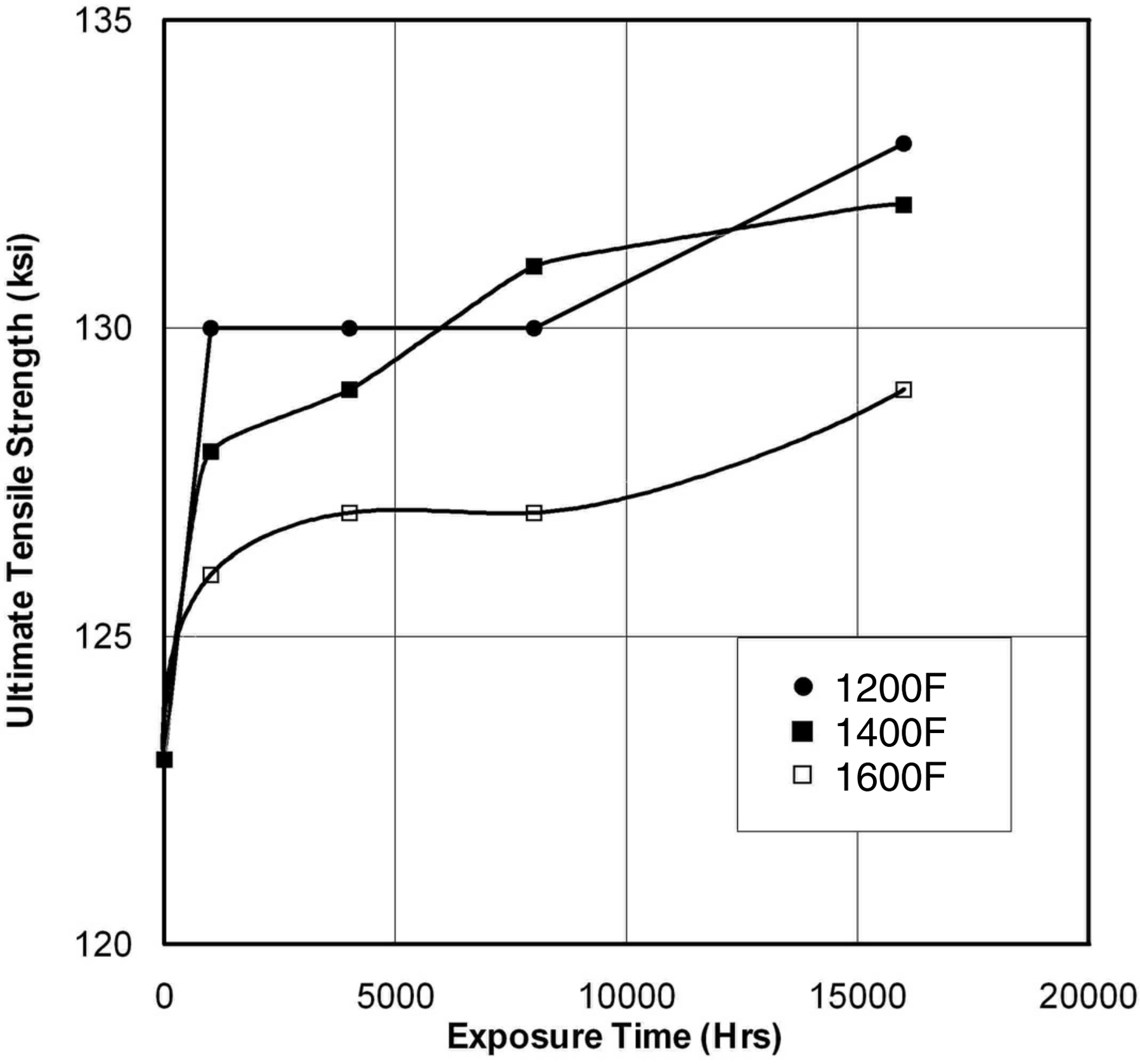

Figure 3.2.1.3 HAYNES 230 alloy: Variation of room temperature ultimate tensile strength with exposure time at 1200F, 1400F and 1600F (Ref. 2)

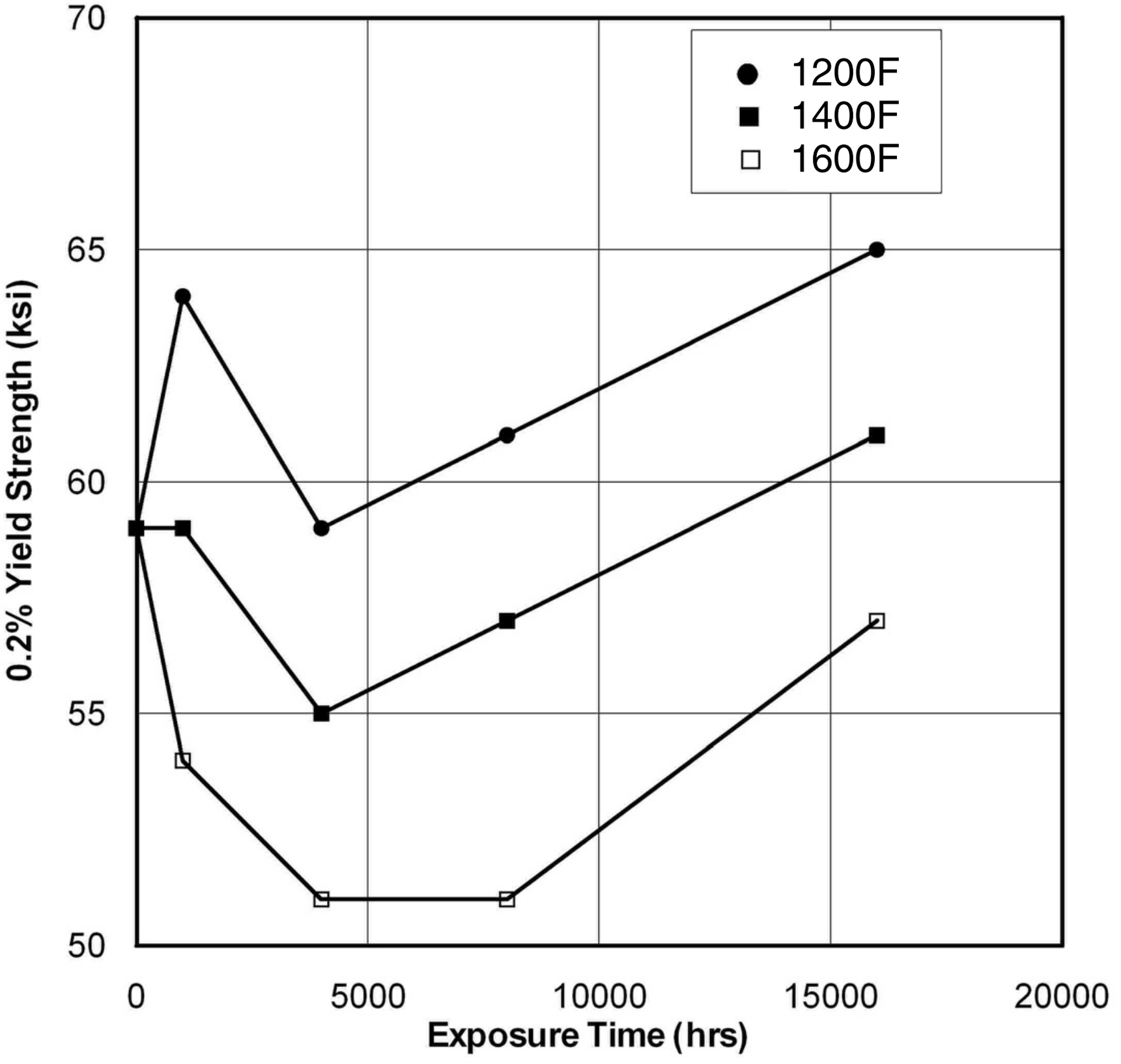

Figure 3.2.1.4 HAYNES 230 alloy: Variation of room temperature 0.2% yield strength with exposure time at 1200F, 1400F, and 1600F (Ref. 2)

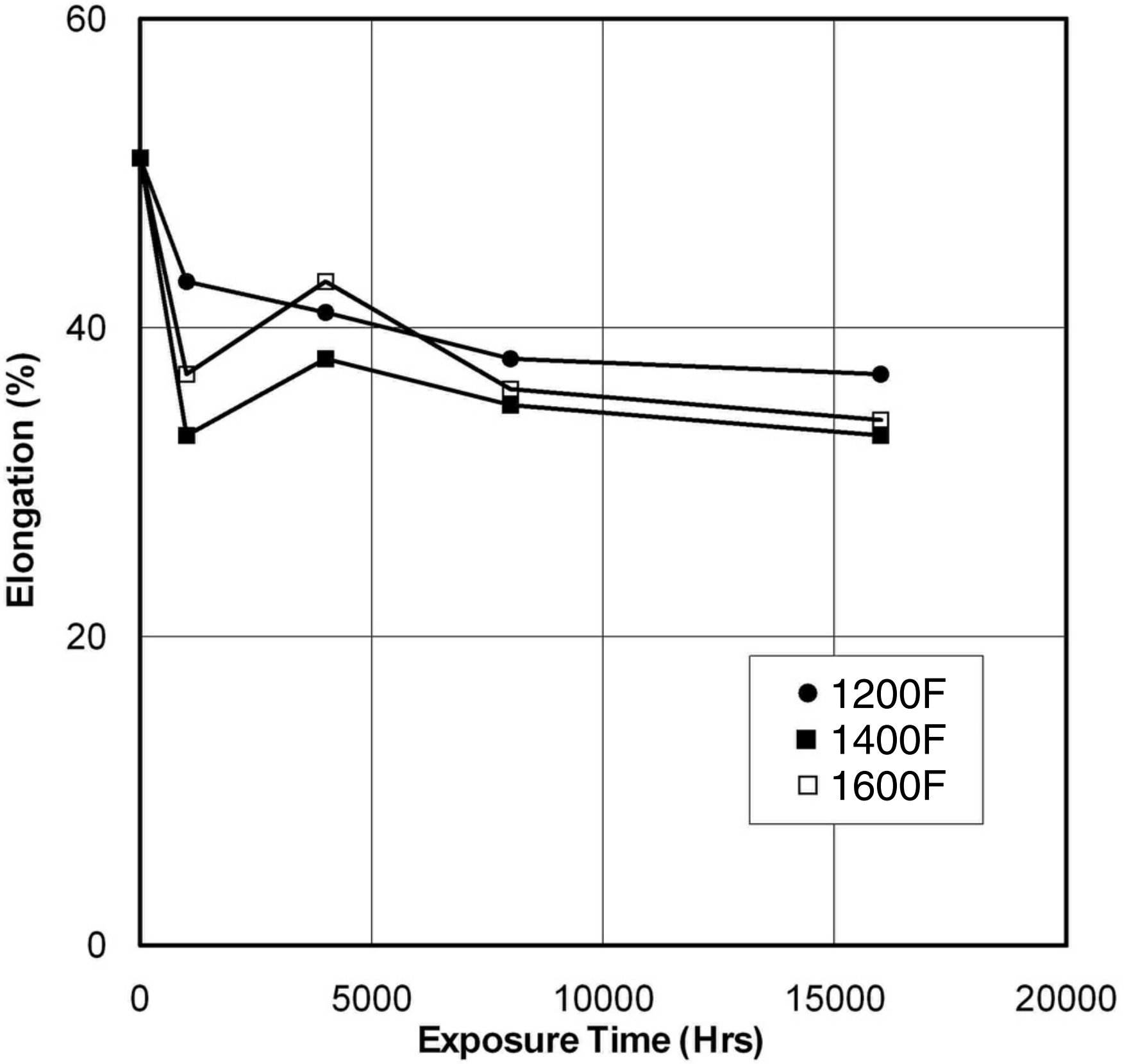

Figure 3.2.1.5 HAYNES 230 alloy: Variation of room temperature tensile elongation with exposure time at 1200F, 1400F, and 1600F (Ref. 2)

Table 3.2.1.6 HAYNES 230 Alloy: Relative change in room temperature tensile properties for samples aged for various times at 932F (500C) and 1022F (550C) (Ref. 10)

Tensile Property	Reference Values	300 hrs % Increase		1000 hrs % Increase		2500 hrs % Increase	
		932F (500C)	1022F (550C)	932F (500C)	1022F (550C)	932F (500C)	1022F (550C)
Ultimate Tensile Strength (ksi (MPa))	125.1 (862)	1	0.9	1	1.3	1.7	1.2
0.1% Yield Strength (ksi (MPa))	53.1 (366)	9.5	9.5	8.7	9.6	10.3	13.3
0.2% Yield Strength (ksi (MPa))	55 (379)	4	3.2	3.9	4.7	5.5	5.6
Elongation (%)	47.8	6.1	12.3	5.9	6	9.8	8.4
Reduction in Area (%)	48	16.2	20	13.2	4.6	16.4	16.3

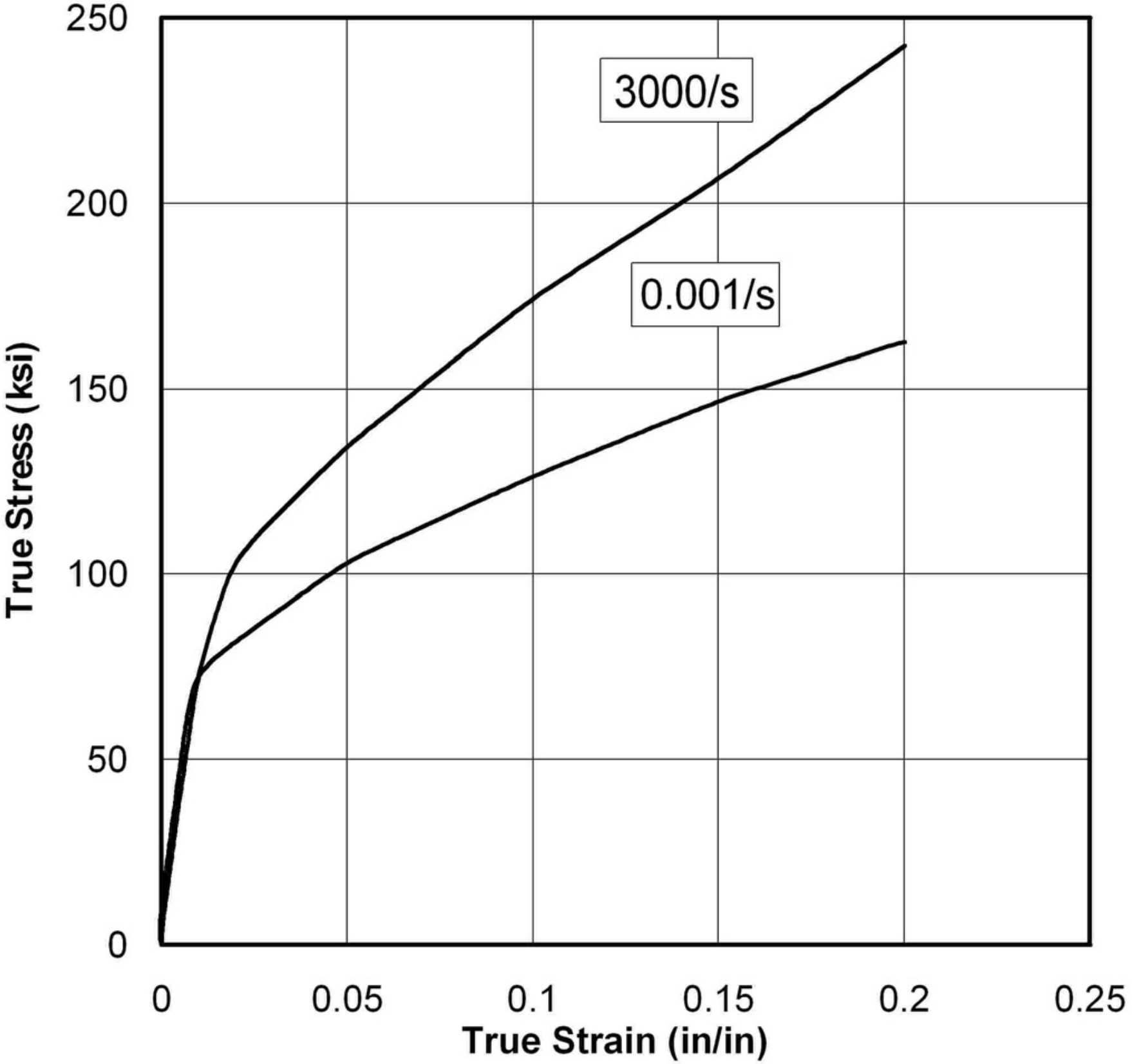

Figure 3.2.2.1 HAYNES 230 alloy: Room temperature compression stress-strain curves at strain rates of 0.001/s and 3000/s (Ref. 29)

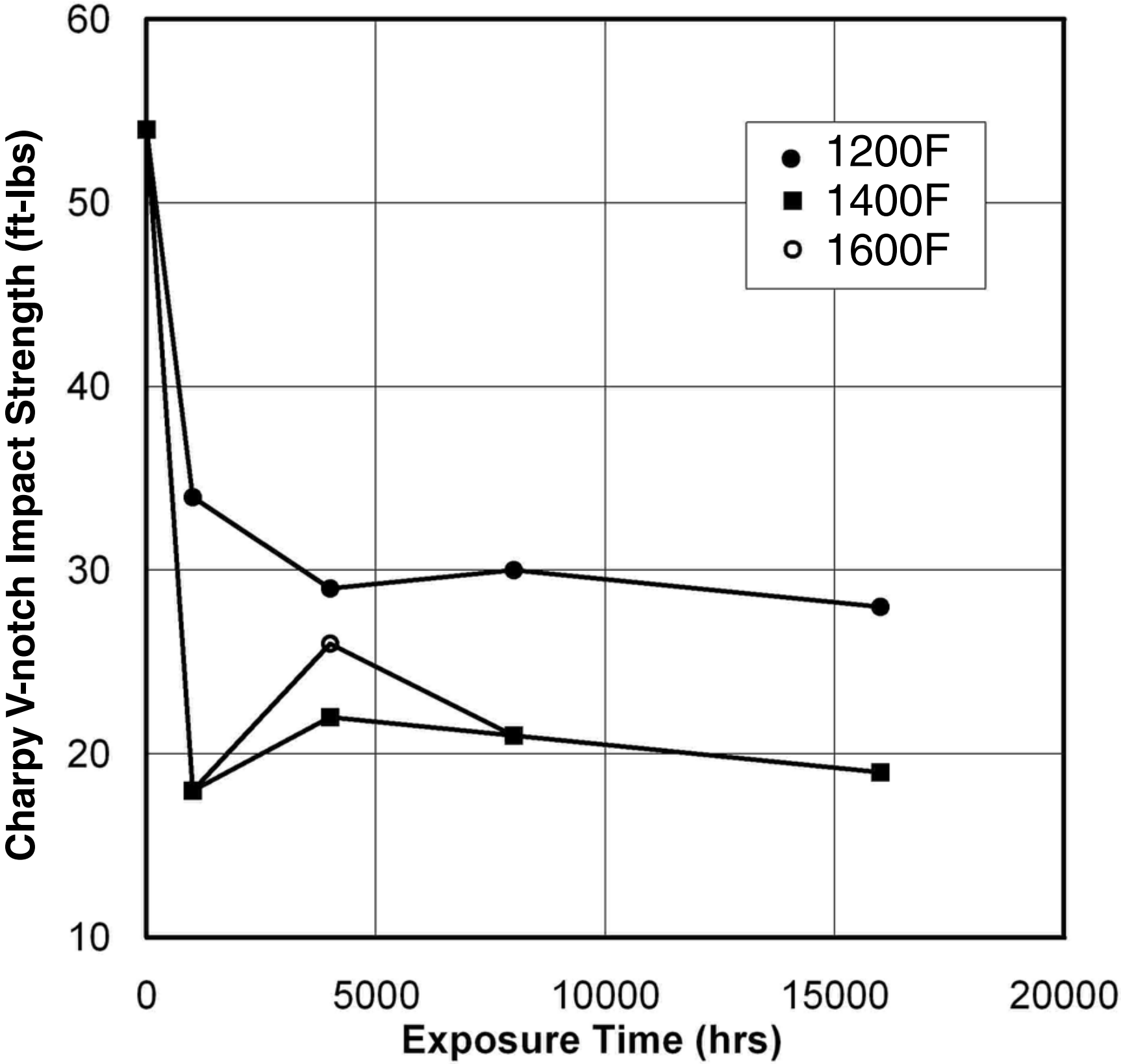

Figure 3.2.3.1 HAYNES 230 alloy: Room temperature Charpy-V impact strength after exposures to 1200F, 1400F and 1600F (Ref. 27)

Table 3.2.3.2 Comparative room temperature Charpy-V impact strengths following 8,000-hour exposures at temperatures of 1200F, 1400F and 1600F for several nickel-base alloys (Ref. 2)

Alloy	Charpy-V Impact Toughness (ft-lbs)			
	Solution Annealed	1200F/8000 hrs	1400F/8000 hrs	1600F/8000 hrs
230	54	30	21	21
625	81	5	5	15
X	54	15	8	15
188	143	23	3	9

Table 3.2.3.3 HAYNES 230 Alloy: Average room temperatureCharpy-V impact strength after aging at 932F (500C) and 1022F (550C) for 1000 hours (Ref. 10)

Aging Temperature	Charpy-V Impact Strength	
	(Ft-lbs)	(Joules)
None	78.4	106.3
932F(500C)	89.3	121
1022F(550C)	102.7	139.2

Table 3.2.7.2.1 HAYNES 230 Alloy: Average room temperature fracture toughness data for 1-inch-thick plate (Ref. 31)

Material Condition	Fracture Toughness (K_{Jq}) (Ksi-in$^{1/2}$)
Solution Annealed	162
Aged at 1400F/4000 hrs.	105.2

Table 3.3.1.1 HAYNES 230 Alloy: Average tensile properties from 77 to -452F for 0.025-0.040-inch-thick sheet (Ref. 25)

Temperature (F)	Ultimate Tensile Strength (ksi)	0.2% Yield Strength (ksi)	Elongation (%)
77	129.4	61.2	44.9
-321	179.8	97.1	45.1
-452	198	122.2	43.5

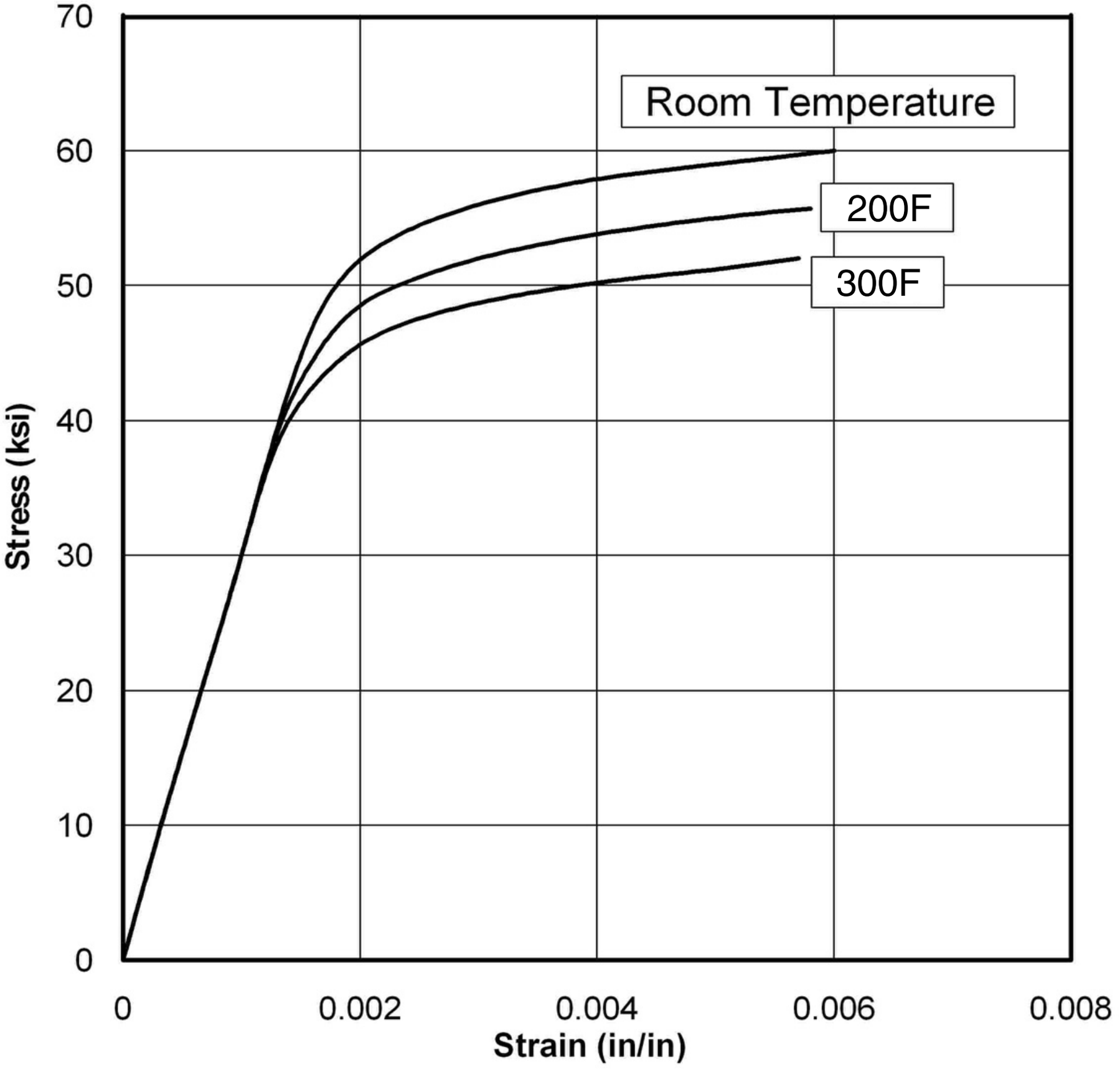

Figure 3.3.1.2 HAYNES 230 alloy: Typical room temperature–300F, LT stress-strain curves for 0.50–0.75-inch-thick plate (Ref. 26)

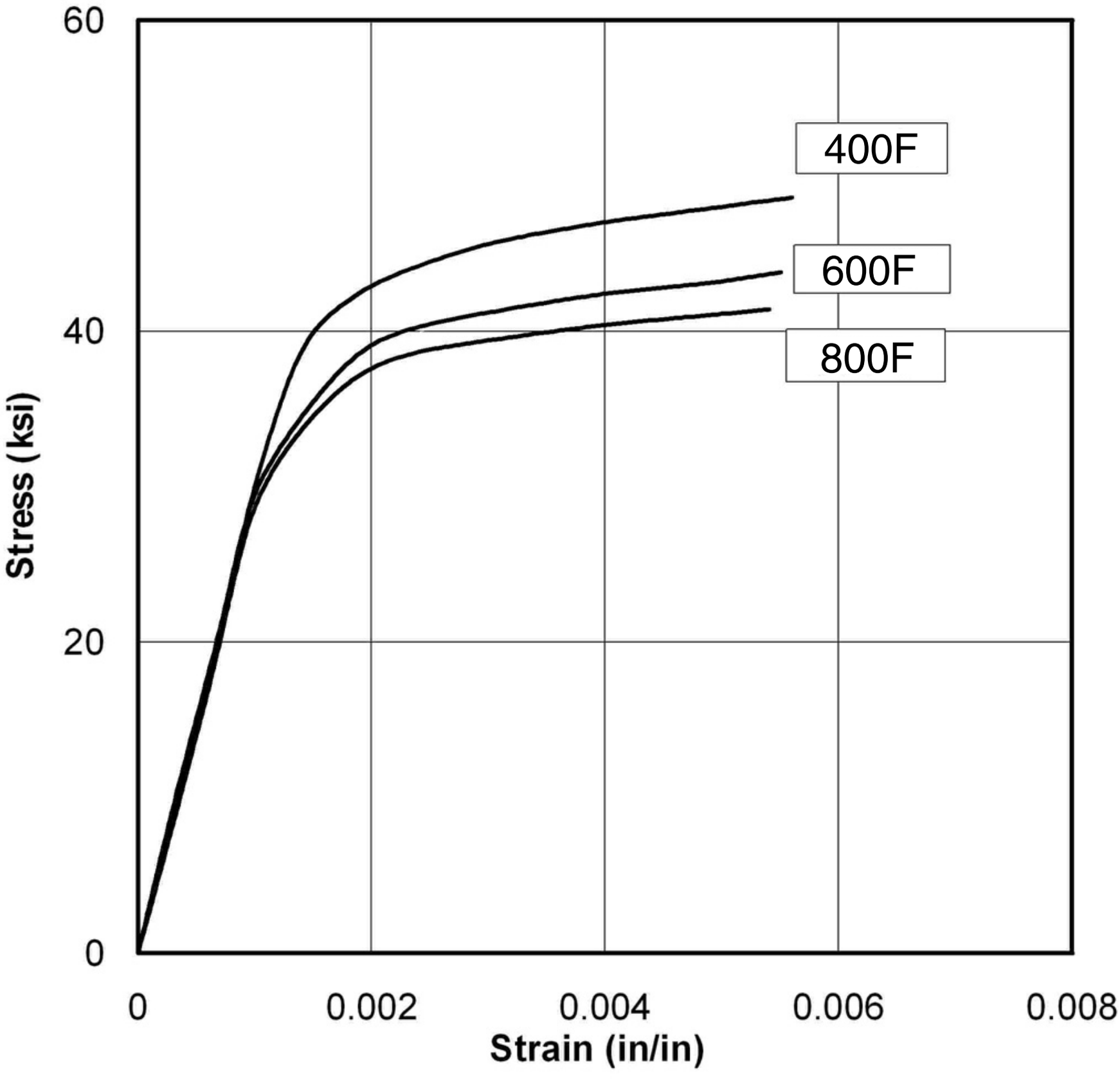

Figure 3.3.1.3 HAYNES 230 alloy: Typical stress-strain curves from 400–800°F for 0.50–0.75-inch-thick plate, LT (Ref. 26)

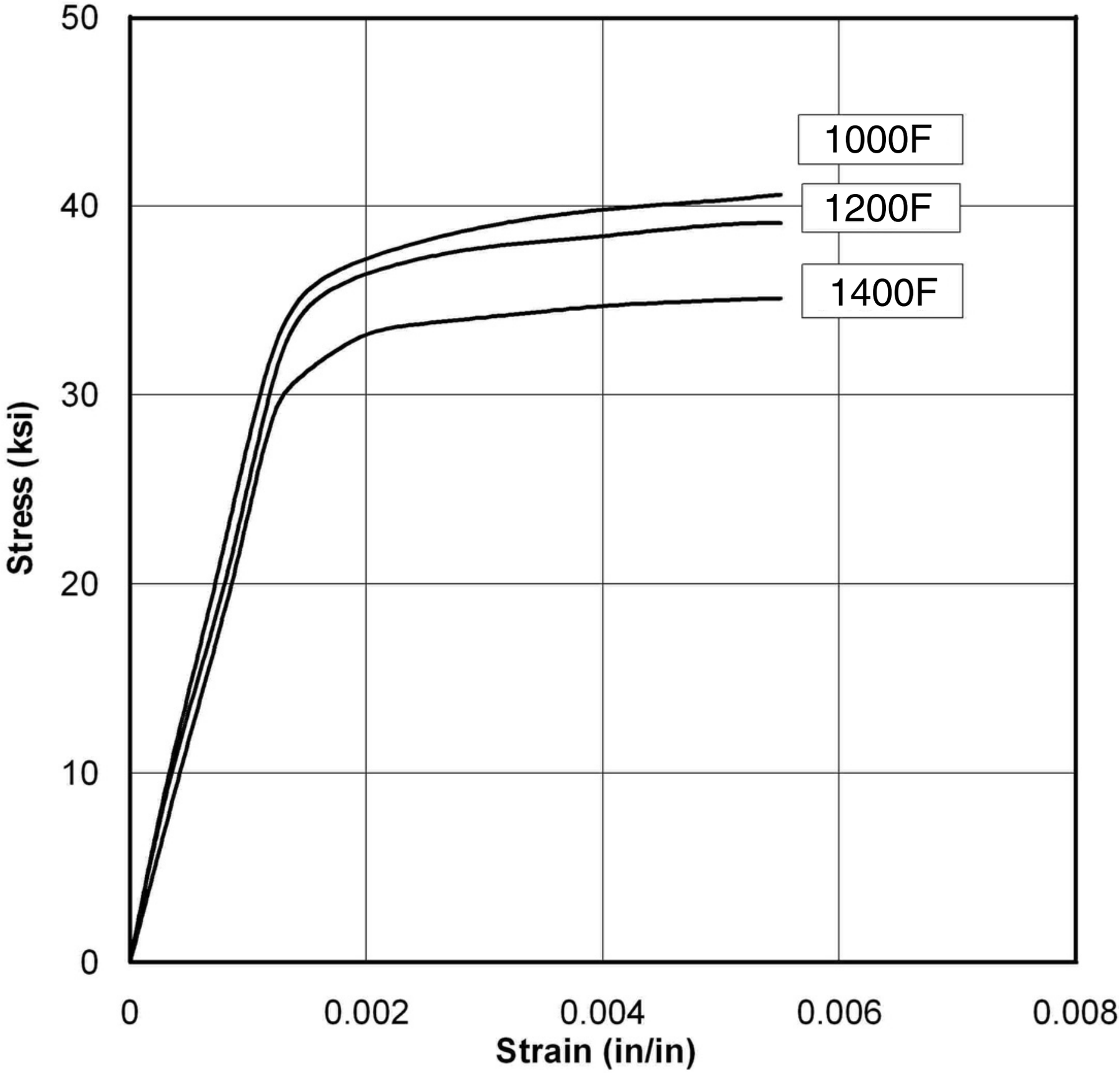

Figure 3.3.1.4 HAYNES 230 alloy: Typical stress-strain curves from 1000–1400F for 0.50–0.75-inch-thick plate, LT (Ref. 26)

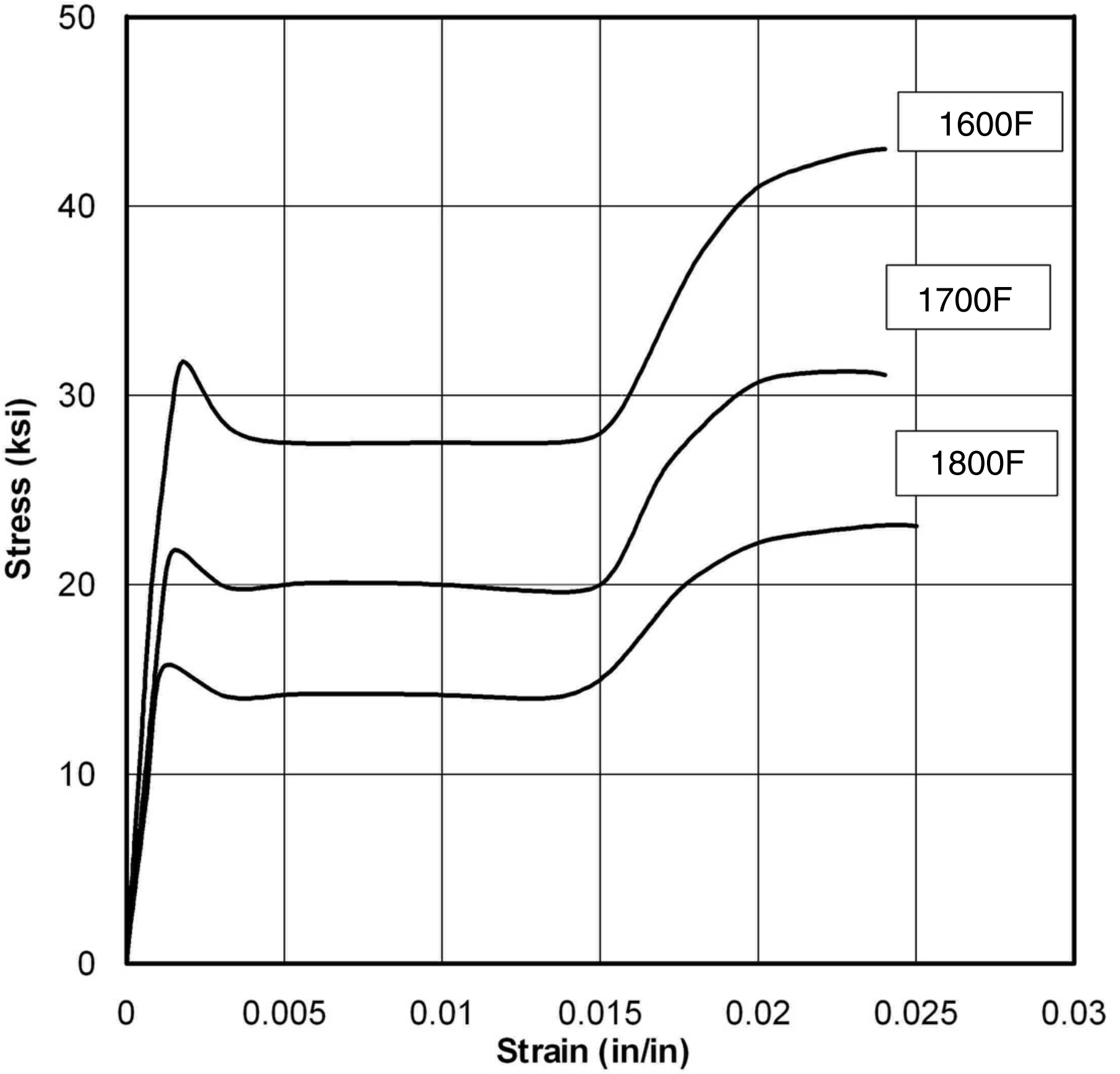

Figure 3.3.1.5 HAYNES 230 alloy: Typical stress-strain curves from 1600–1800°F for 0.50–0.75-inch-thick plate, LT (Ref. 26)

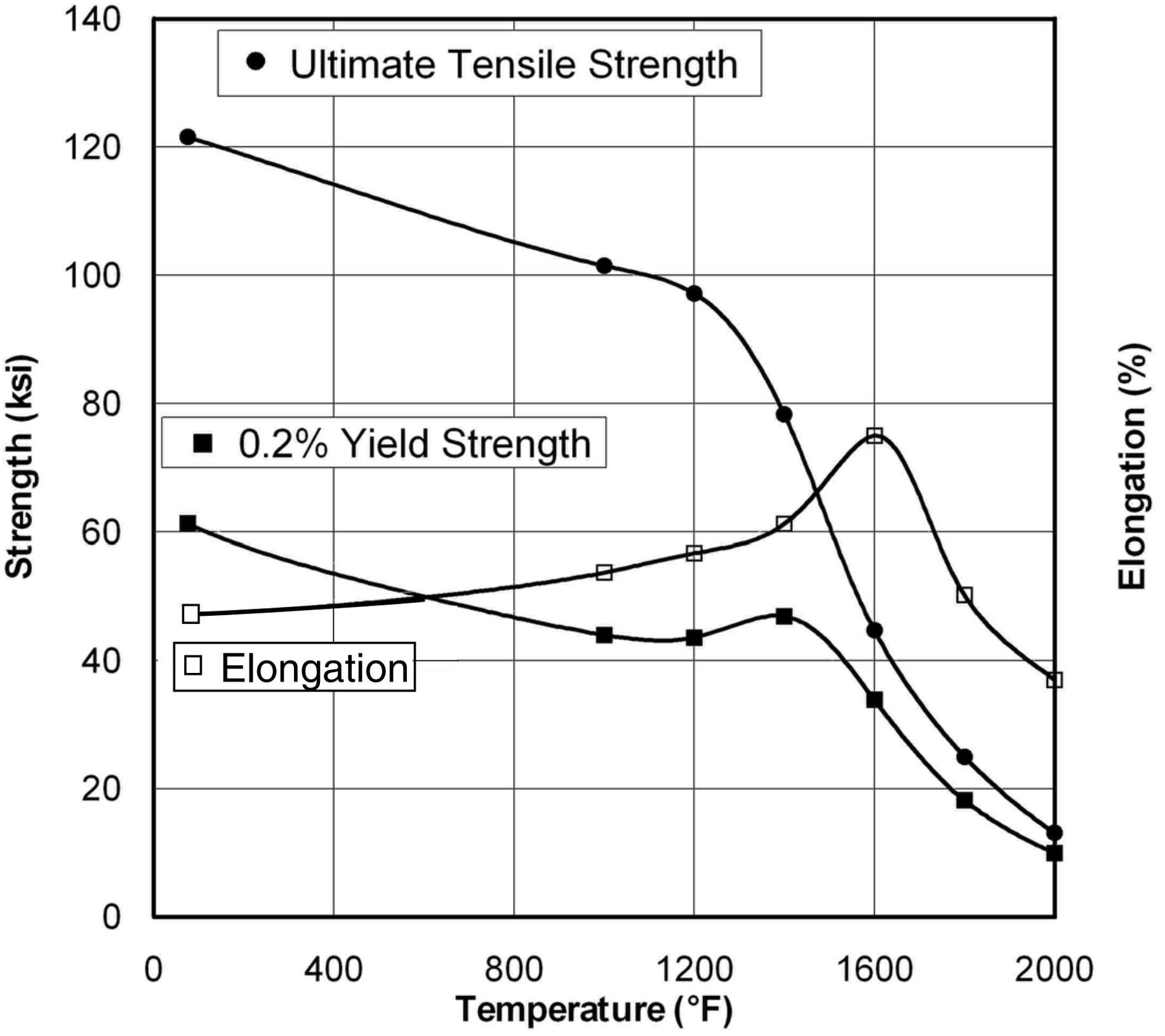

Figure 3.3.1.6 HAYNES 230 alloy: Tensile properties for sheet from room temperature to 2000F (Ref. 2)

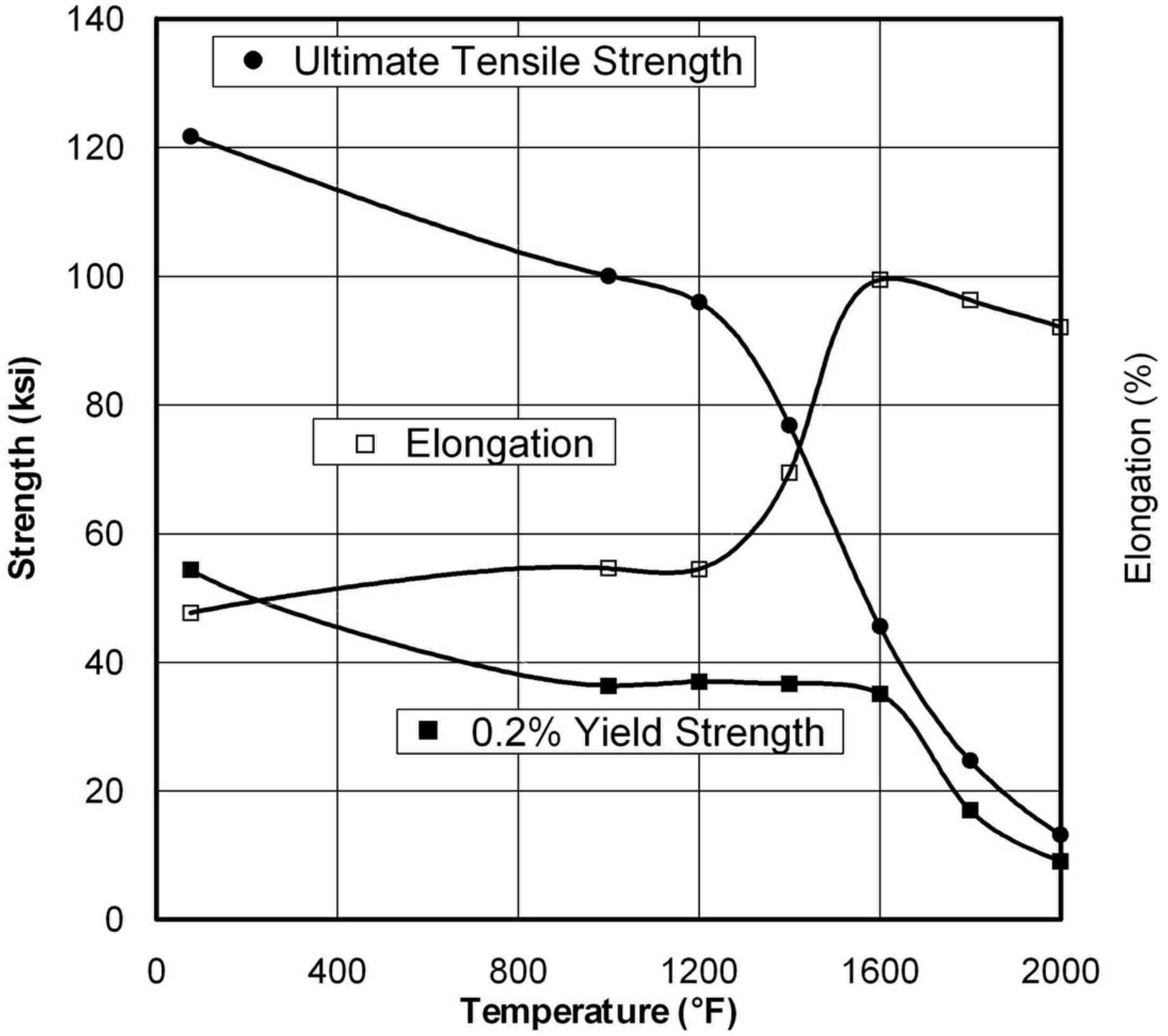

Figure 3.3.1.7 HAYNES 230 alloy: Tensile properties for plate from room temperature to 2000F (Ref. 2)

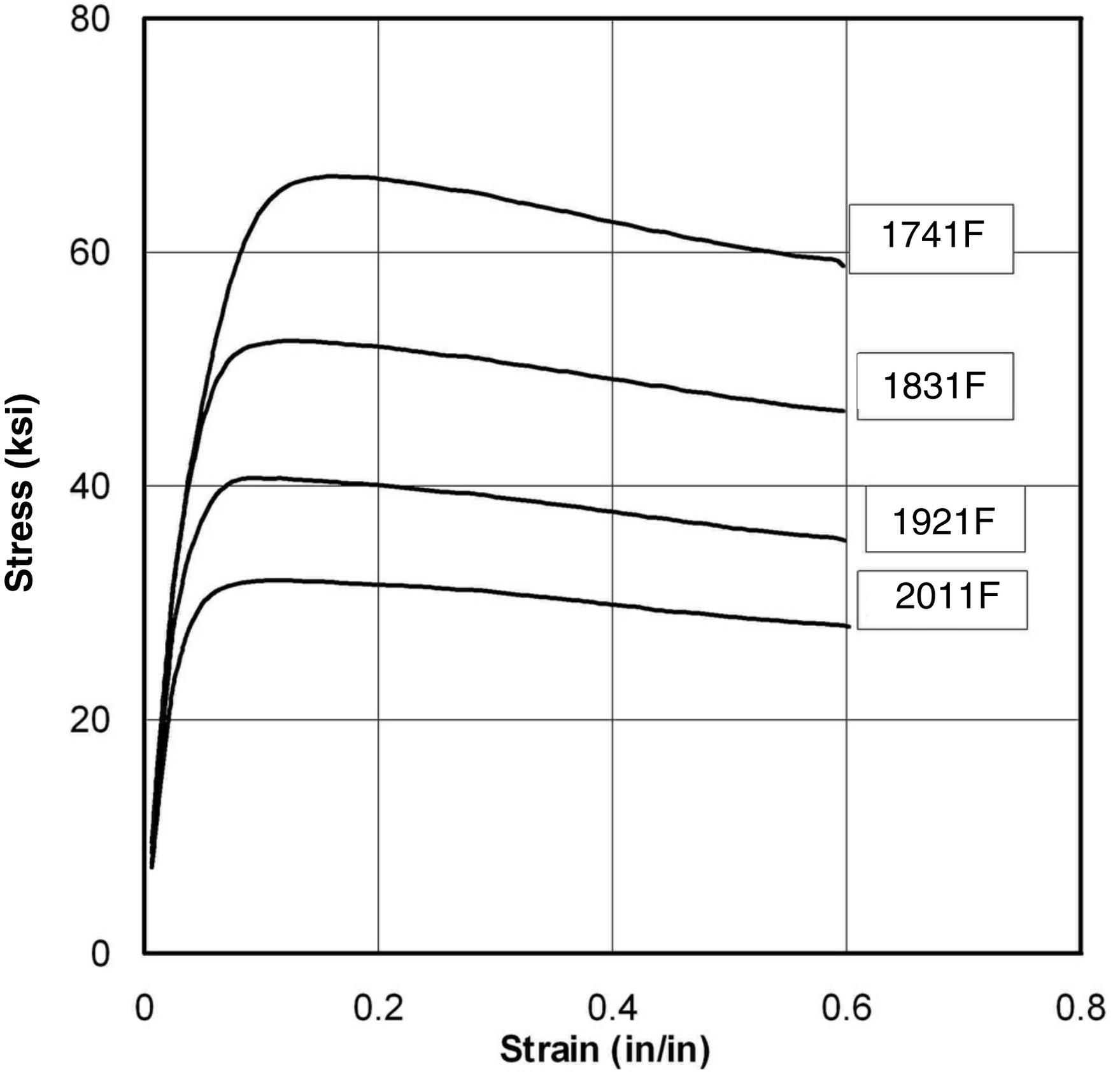

Figure 3.3.2.1 HAYNES 230 alloy: Compression stress-strain curves from 1741–2011F at a strain rate of 0.1/s (Ref. 30)

Table 3.4.1 HAYNES 230 Alloy: Creep and rupture properties of solution-annealed sheet (Ref. 2)

Test Temperature (F (C))	Creep Strain (%)	Approximate Initial Stress to Produce Specified Creep Strain in Indicated Time (ksi (MPa))			
		10 hrs	100 hrs	1000 hrs	10,000 hrs
	0.5	48.0 (330)	32.0 (220)	22.0 (150)	-
	1	51.0 (350)	36.0 (250)	25.0 (170)	-
1200 (649)	Rupture	67.0 (460)	48.0 (330)	36.0 (250)	27.0 (185)
	0.5	31.0 (215)	21.3 (145)	14.5 (100)	-
	1	34.0 (235)	24.0 (165)	16.5 (115)	-
1300 (704)	Rupture	47.0 (325)	34.0 (235)	25.0 (170)	18.5 (130)
	0.5	17.2 (120)	13.7 (95)	10.8 (75)	-
	1	20.0 (140)	14.8 (100)	11.7 (81)	-
1400 (760)	Rupture	32.0 (220)	24.5 (170)	18.2 (125)	13.2 (91)
	0.5	13.1 (90)	10.3 (71)	7.8 (54)	-
	1	14.1 (97)	11.2 (77)	8.6 (59)	-
1500 (816)	Rupture	23.3 (160)	17.5 (120)	12.5 (86)	8.4 (58)
	0.5	10.0 (69)	7.6 (52)	5.5 (38)	-
	1	11.0 (76)	8.4 (58)	5.8 (40)	-
1600 (871)	Rupture	17.0 (115)	12.1 (83)	8.2 (57)	5.6 (39)
	0.5	7.5 (52)	5.4 (37)	3.4 (23)	-
	1	8.3 (57)	5.7 (39)	3.6 (25)	-
1700 (927)	Rupture	12.0 (83)	8.0 (55)	4.9 (34)	3.2 (22)
	0.5	5.4 (37)	3.4 (23)	1.7 (12)	-
	1	5.7 (39)	3.6 (25)	1.9 (13)	-
1800 (982)	Rupture	8.0 (55)	4.9 (34)	2.6 (18)	1.1 (7.6)
	0.5	-	-	-	-
	1	-	-	-	-
1900 (1038)	Rupture	7.5 (52)	3.5 (24)	1.6 (11)	-

Table 3.4.2 HAYNES 230 Alloy: Creep and rupture properties of solution-annealed bar and plate (Ref. 2)

Test Temperature (F (C))	Creep Strain (%)	Approximate Initial Stress to Produce Specified Creep Strain in Indicated Time (ksi (MPa))			
		10 hrs	100 hrs	1000 hrs	10,000 hrs
	0.5	59.0 (405)	34.0 (235)	23.0 (160)	-
	1	60.0 (415)	39.0 (270)	26.4 (180)	17.5 (120)
1200 (649)	Rupture	-	56.0 (385)	42.5 (295)	29.0 (200)
	0.5	30.0 (205)	20.5 (140)	15.0 (105)	-
	1	35.0 (240)	23.5 (160)	18.0 (125)	12.3 (85)
1300 (704)	Rupture	52.0 (360)	39.0 (270)	29.0 (200)	21.0 (145)
	0.5	19.0 (1300	14.0 (97)	11.0 (76)	-
	1	21.5 (150)	15.9 (110)	11.5 (79)	8.0 (55)
1400 (760)	Rupture	37.0 (255)	27.0 (185)	20.0 (140)	14.2 (98)
	0.5	13.4 (92)	10.6 (73)	8.2 (57)	-
	1	15.0 (105)	12.0 (83)	9.2 (63)	6.5 (45)
1500 (816)	Rupture	26.0 (180)	19.0 (130)	14.0 (97)	9.8 (68)
	0.5	10.3 (71)	8.0 (55)	5.6 (39)	-
	1	11.7 (81)	9.0 (62)	6.0 (41)	4.4 (30)
1600 (871)	Rupture	18.8 (130)	13.7 (95)	9.5 (66)	6.2 (430)
	0.5	7.8 (54)	5.5 (38)	3.4 (23)	-
	1	8.8 (61)	6.3 (43)	4.0 (28)	2.6 (18)
1700 (927)	Rupture	13.4 (92)	9.4 (65)	6.0 (41)	3.5 (24)
	0.5	5.5 (38)	3.4 (23)	1.6 (11)	-
	1	6.3 (43)	3.8 (26)	2.0 (14)	1.1 (7.6)
1800 (982)	Rupture	9.4 (65)	6.0 (41)	3.0 (21)	1.6 (11)
	0.5	-	-	-	-
	1	4.4 (30)	2.0 (14)	0.9 (6.2)	-
1900 (1038)	Rupture	7.0 (48)	3.5 (24)	1.8 (12)	-
	0.5	-	-	-	-
	1	2.3 (16)	0.8 (5.5)	-	-
2000 (1093)	Rupture	4.2 (29)	2.1 (14)	1.0 (6.9)	-
	0.5	-	-	-	-
	1	1.1 (7.6)	0.4 (2.8)	-	-
2100 (1149)	Rupture	2.3 (16)	1.2 (8.3)	0.6 (4.1)	-

Table 3.4.3 Effects of thermomechanical cycles on 1600°F (871°C)/7 ksi (48 MPa) creep properties for several nickel-base alloys (Ref. 32)

Alloy	Time to Indicated Creep Strain (hrs)					
	As-Received		10% Strain + Indicated Heat Treatment*			
			1900F (1038C)		2050F (1121C)	
	0.50%	1.00%	0.50%	1.00%	0.50%	1.00%
X	13	26	93	182	5	12
188	162	334	549	>1000**	680	>900**
230	88	221	1035	>1510**	50	150
617	66	160	840	>1510**	50	150
86	18	26	310	595	5	13

*5-15 min. at temperature/air cool

** Test discontinued

Table 3.4.4 Effects of secondary heat treatments on 1600F (871C)/7 ksi (48 MPa) creep properties for several nickel-base alloys (Ref. 32)

	Time to Indicated Creep Strain (hrs)							
			Secondary Heat Treatment*					
	As-Received		1900F (1038C)		2050F (1121C)		2150F (1177C)	
Alloy	0.50%	1.00%	0.50%	1.00%	0.50%	1.00%	0.50%	1.00%
X	13	26	7	16	6	14	7	24
188	162	334	68	200	72	272	97	260
230	88	221	23	52	9	20	20	44
617	66	160	28	71	8	35	15	63
86	18	26	3	9	13	25	10	28

*5-15 min. at temperature/air cool

Table 3.4.5 HAYNES 230 Alloy: Average 1700F (927C)/9 ksi (62 MPa) stress-rupture data for 230 alloy plate for the as-received, exposed and rejuvenated conditions (Ref. 33)

Material Condition	Rupture Life (hrs)	EL (%)	R.A. (%)
AMS 5878A (Minimums)	36	10	-
As-Received	86.2	62.6	65.1
Exposed at 1400F(760C)/1500 hrs.	126.3	53.5	61.4
Exposed at 1600F(871C)/1500 hrs.	102	61.5	67.5
Exposed at 1400F(760C)/1500 hrs. + 2150F(1177C)/0.5 hr./RAC	101.5	64.8	69.7
Exposed at 1600F(871C)/1500 hrs. + 2150F(1177C)/0.5 hr./RAC	94.8	66.4	71.4

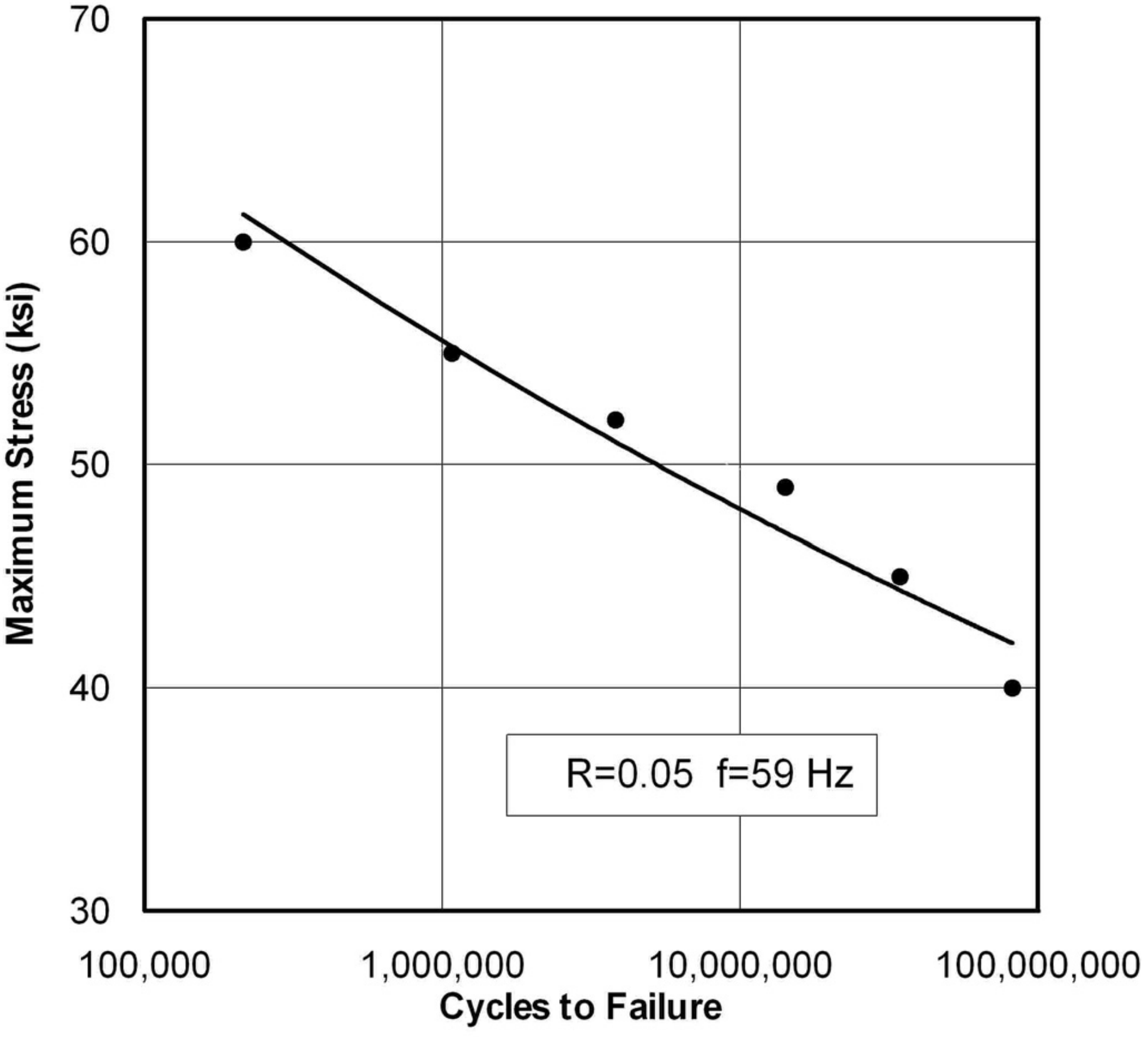

Figure 3.5.1.1 HAYNES 230 alloy: High-cycle fatigue behavior of 0.75-inch-thick plate at 1400F (Ref. 34)

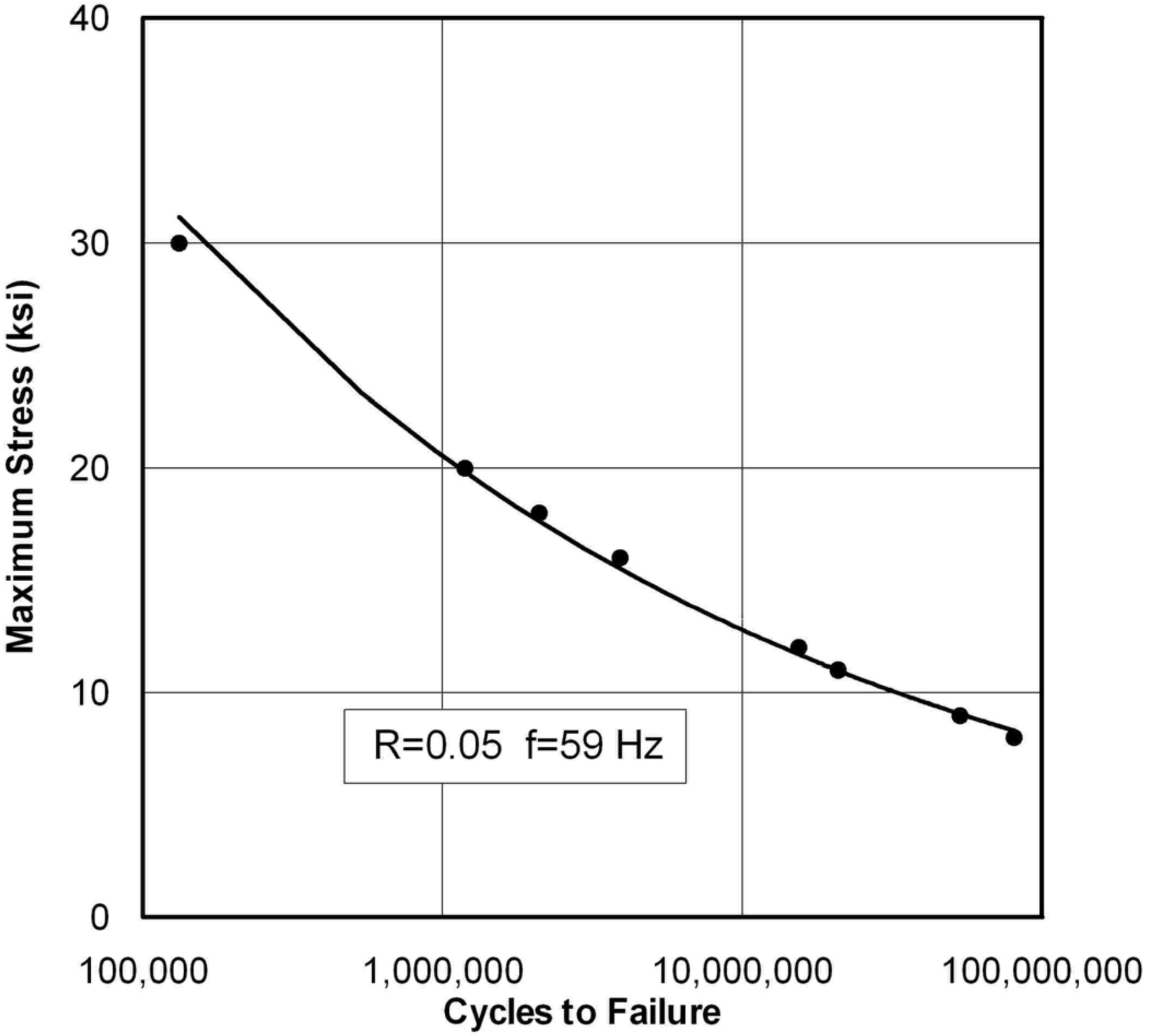

Figure 3.5.1.2 HAYNES 230 alloy: High-cycle fatigue behavior of 0.75-inch-thick plate at 1800F (Ref. 34)

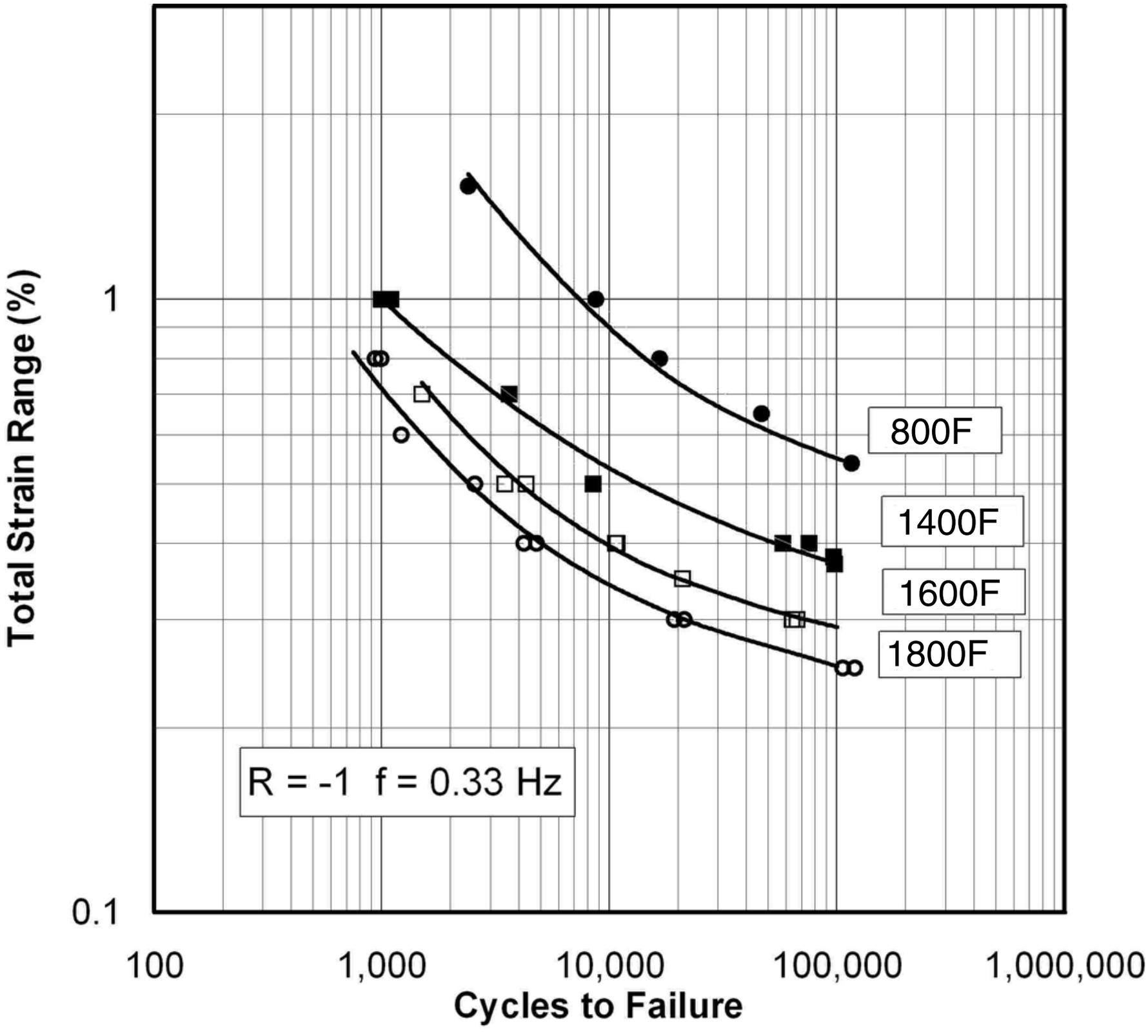

Figure 3.5.2.1 HAYNES 230 alloy: Low-cycle fatigue properties for 0.625-inch-thick plate at elevated temperatures (Refs. 34, 35)

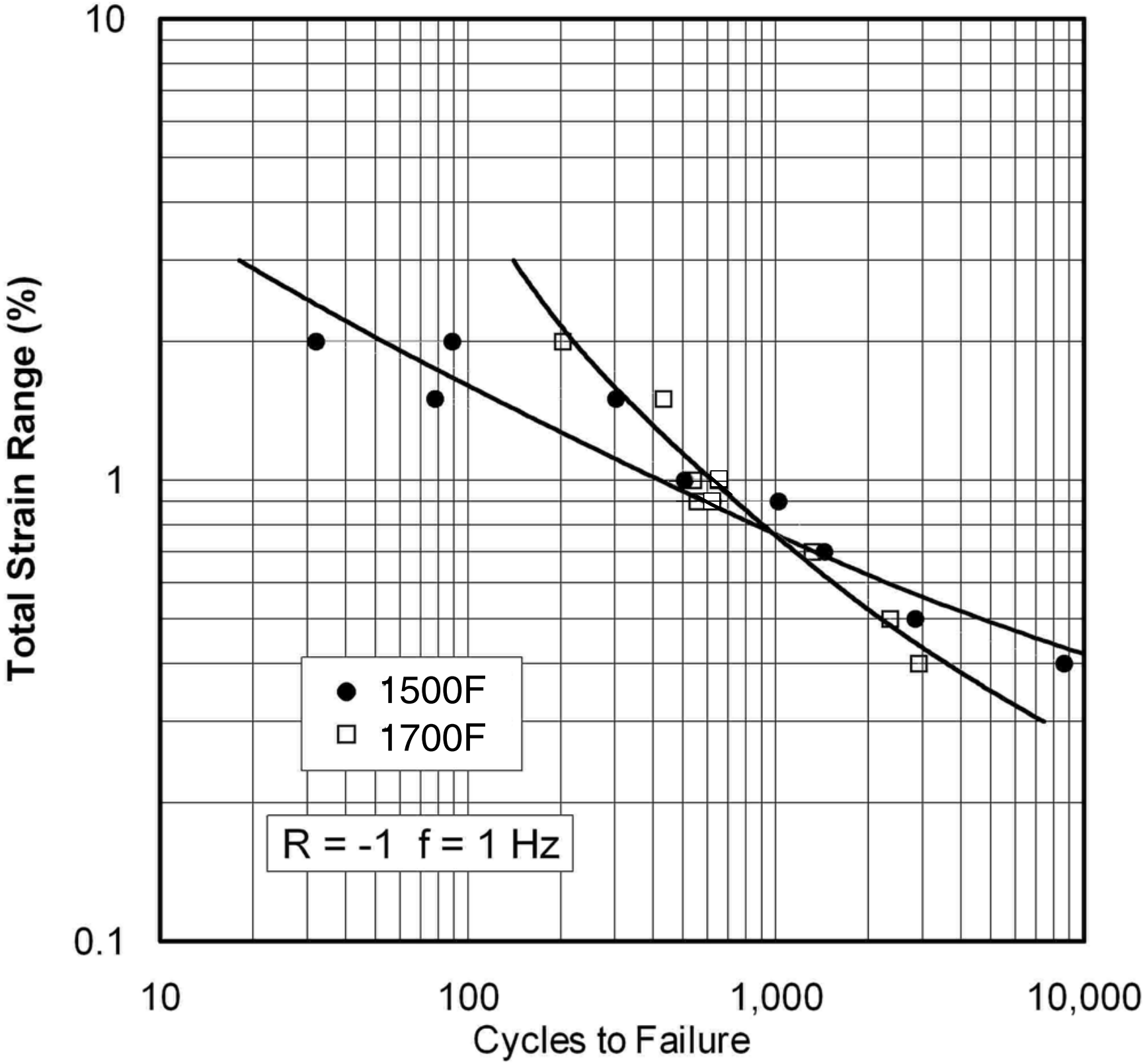

Figure 3.5.2.2 HAYNES 230 alloy: Low-cycle fatigue behavior of 0.125-inch-thick sheet at elevated temperatures (Ref. 36)

Table 3.5.2.3 Effect of aging at 1400F/1000 hours on the 800F low-cycle fatigue lives of several solid-solution-strengthened superalloys (plate and bar samples, R = -1, f = 0.33 Hz) (Ref. 37)

Nominal Strain Range (%)	Ratio of Aged/Annealed Cycles to Failure		
	X	230	188
1.5	0.86	0.94	0.77
1	0.63	0.8	0.55
0.8	0.72	0.92	0.59
0.65	0.75	0.74	0.65
0.55	0.97	1.07	-

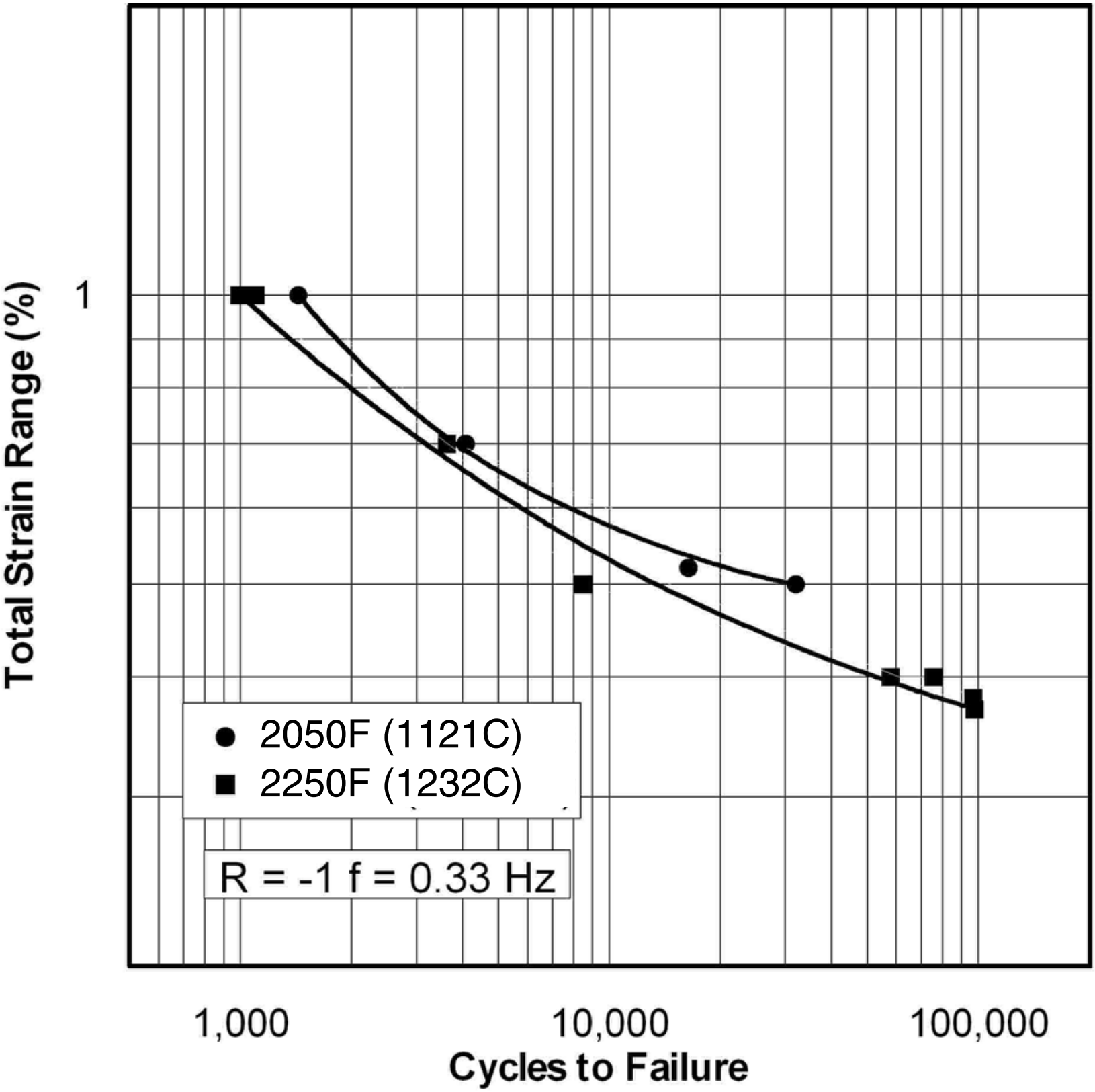

Figure 3.5.2.4 HAYNES 230 alloy: Effect of processing temperature on the 1400F low-cycle fatigue behavior of 0.75-inch-diameter bar (Ref. 38)

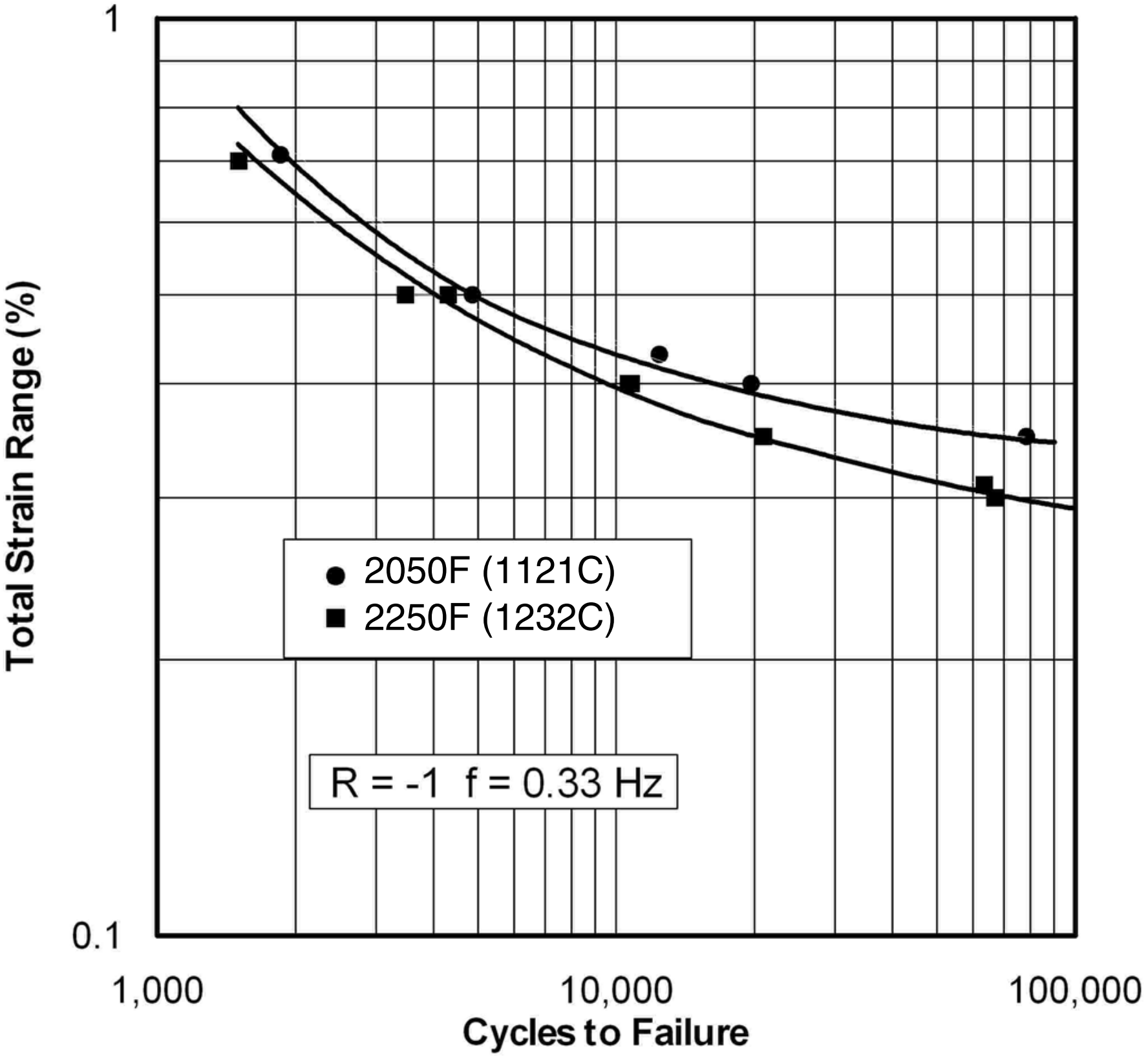

Figure 3.5.2.5 HAYNES 230 alloy: Effect of processing temperature on the 1600F low-cycle fatigue behavior of 0.75-inch-diameter bar (Ref. 38)

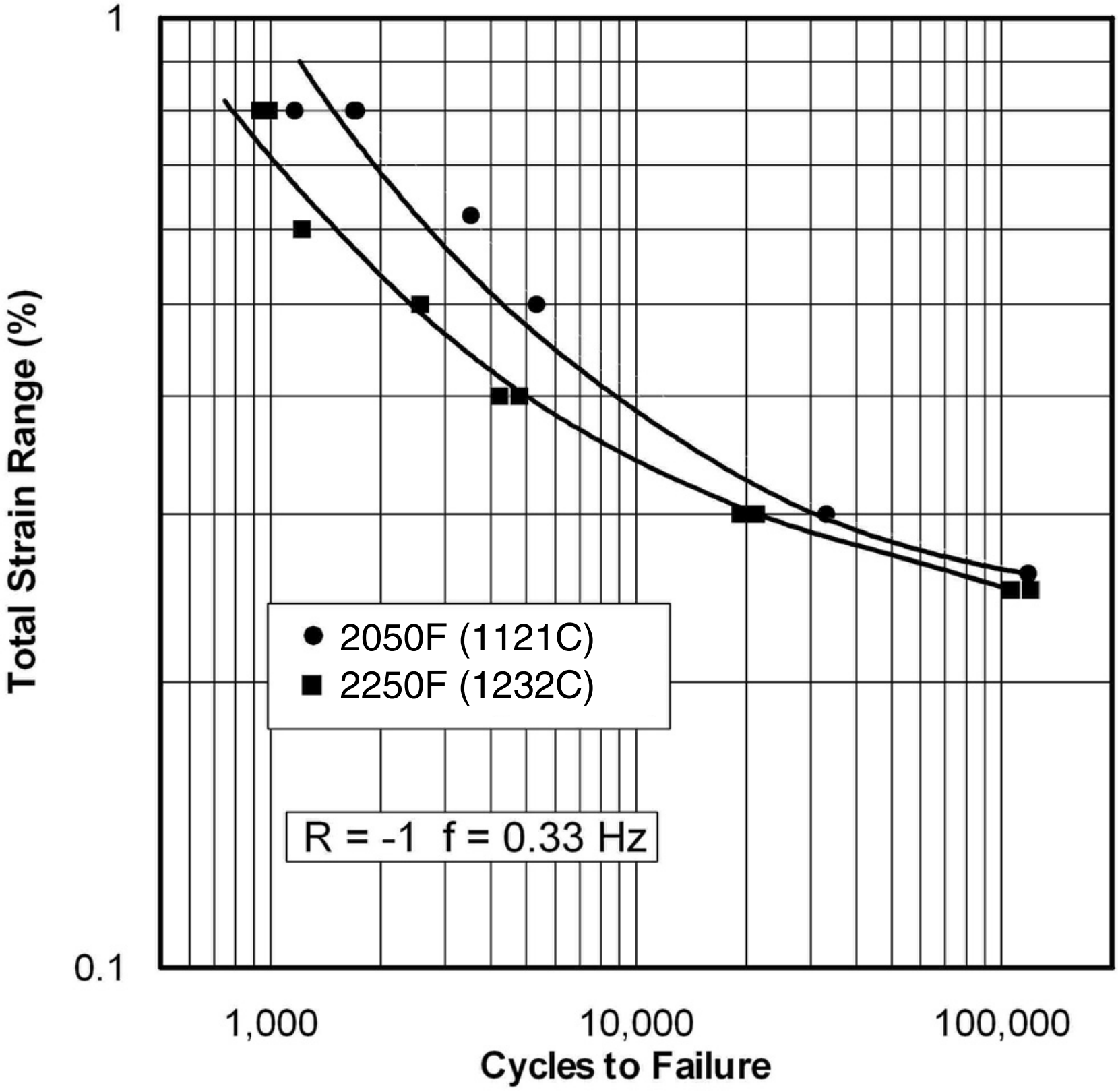

Figure 3.5.2.6 HAYNES 230 alloy: Effect of processing temperature on the 1800F low-cycle fatigue behavior of 0.75-inch-diameter bar (Ref. 38)

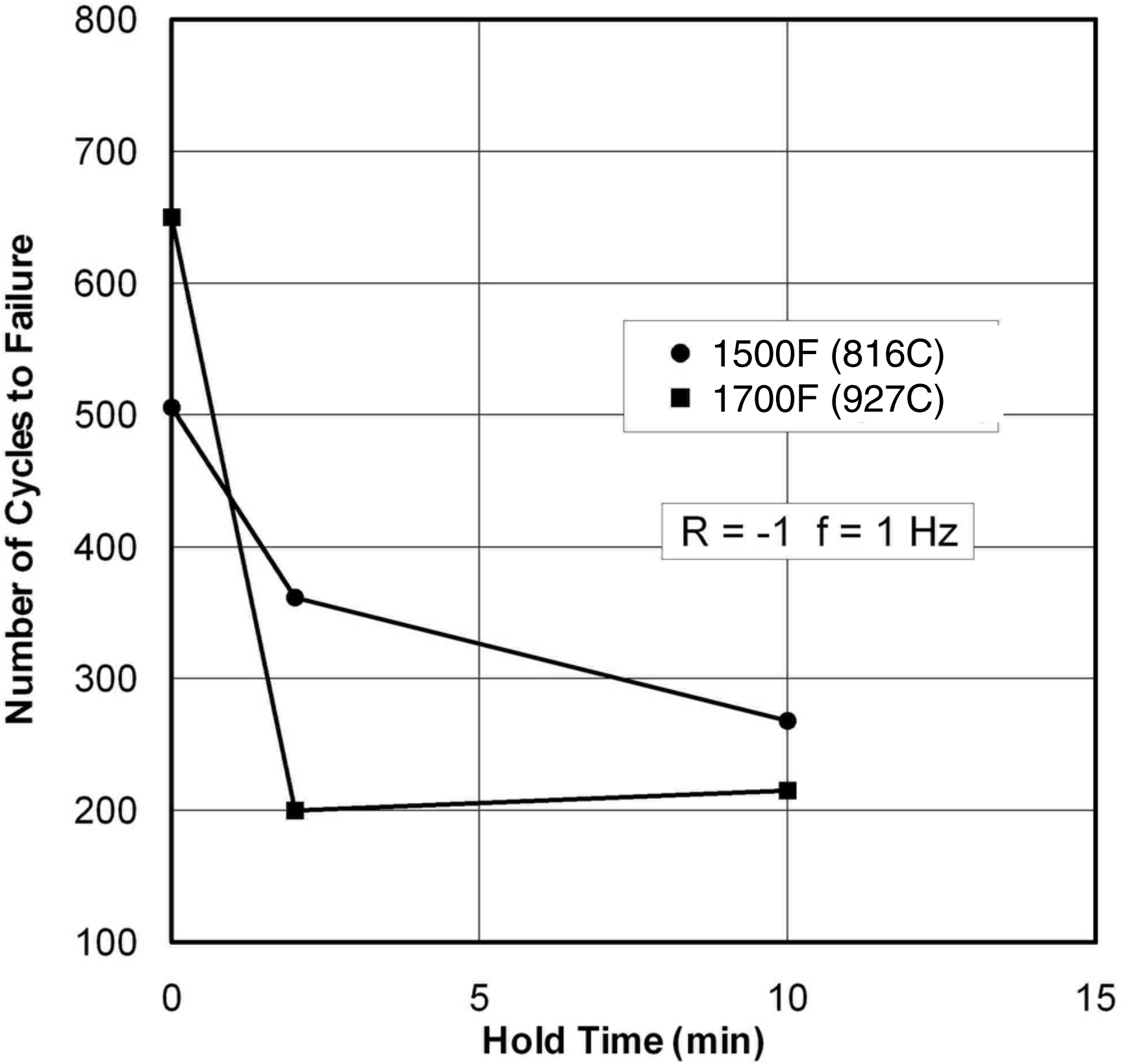

Figure 3.5.2.7 HAYNES 230 alloy: Effect of tensile hold times on the fatigue lives of 0.125-inch-thick sheet at a total strain range of 1.0% (Ref. 39)

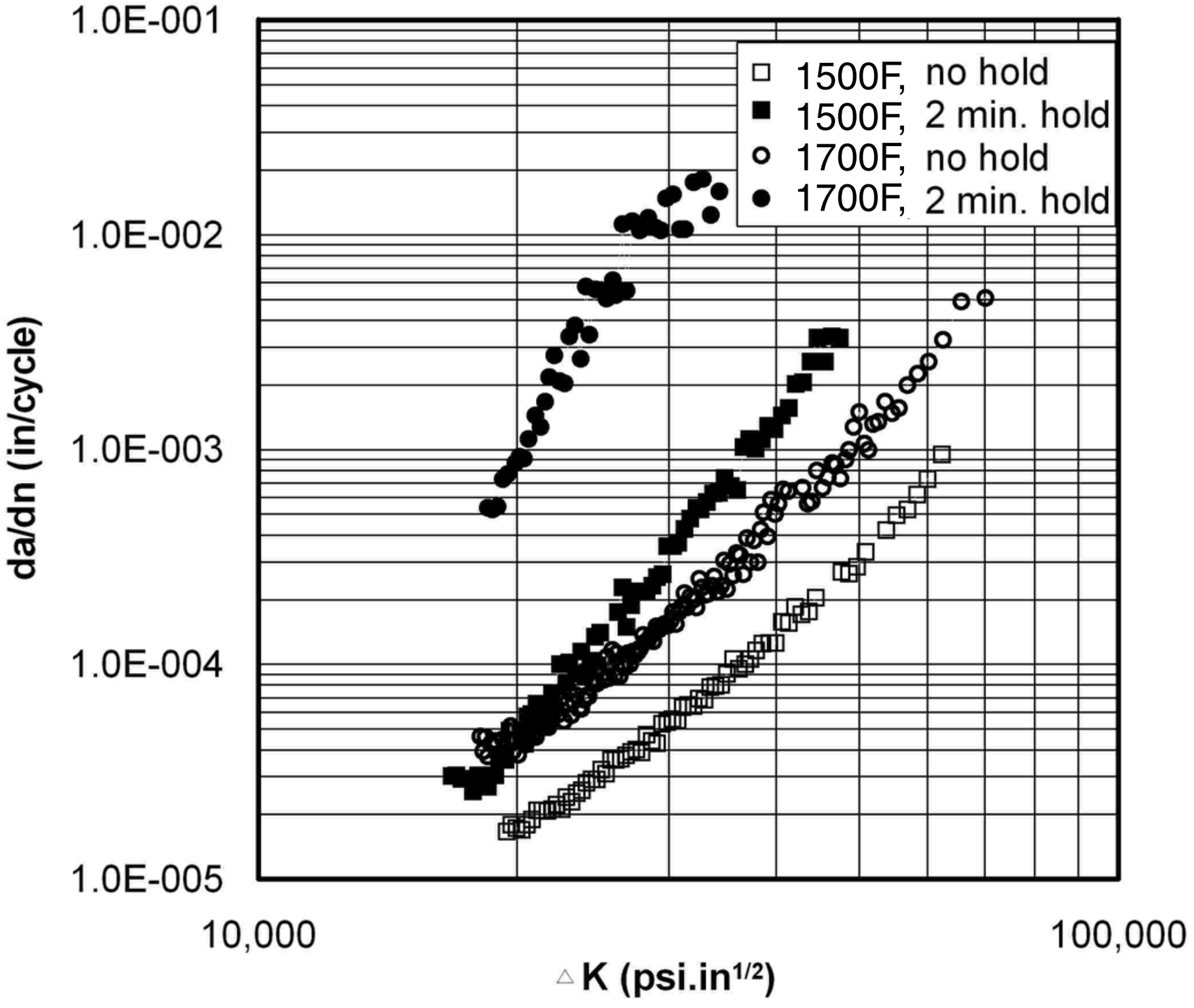

Figure 3.5.3.1 HAYNES 230 alloy: Fatigue crack growth with and without 2-minute tensile holds at 1500F and 1700F (Ref. 40)

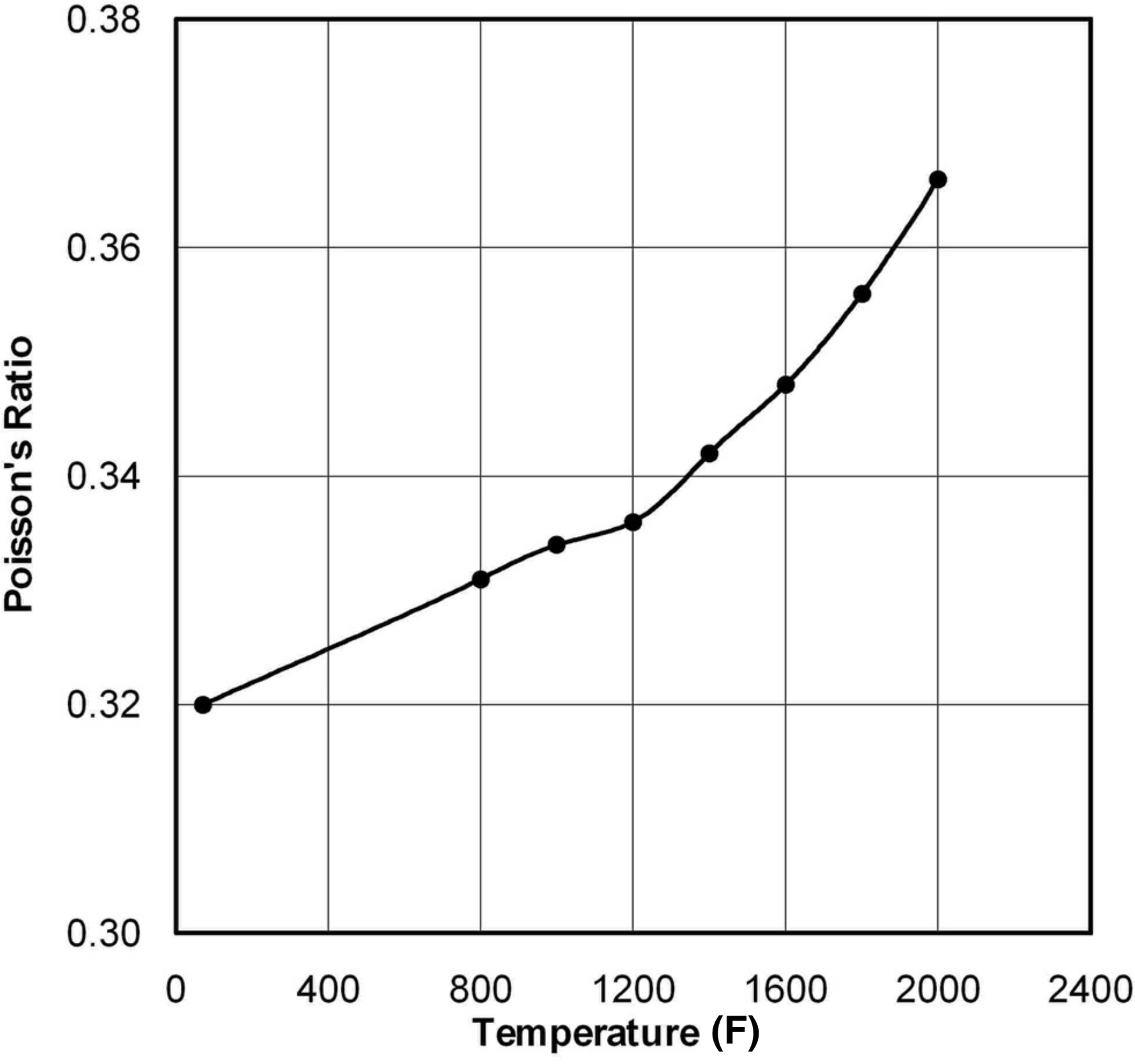

Figure 3.6.1.1 HAYNES 230 alloy: Effect of temperature on Poisson's ratio (Ref. 41)

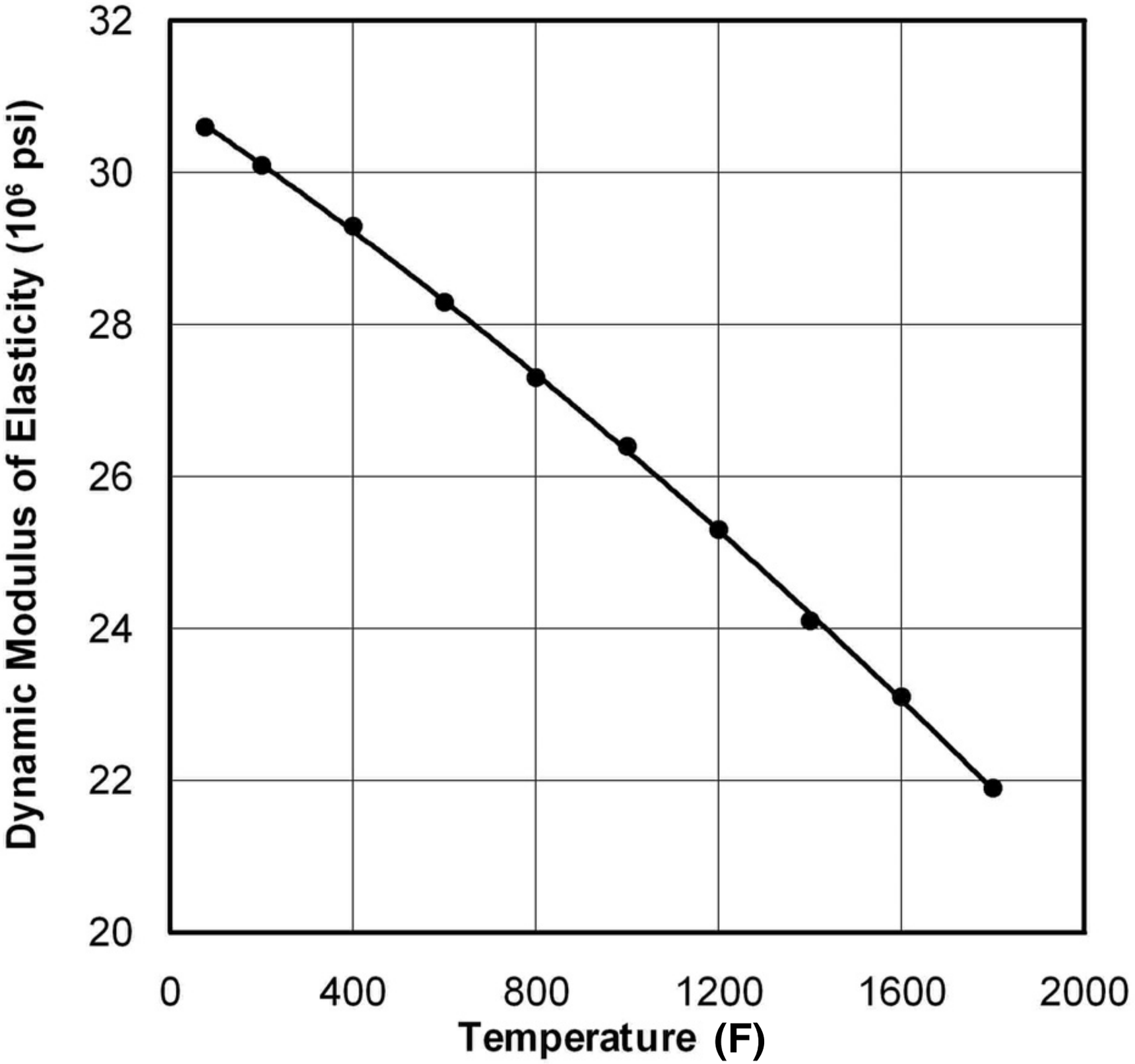

Figure 3.6.2.1 HAYNES 230 alloy: Effect of temperature on the dynamic modulus of elasticity (Ref. 2)

Table 4.3.1 Tensile properties for GMAW deposits of HAYNES 230-W weld metal (Ref. 2)

Test Temperature (F)	Ultimate Tensile Strength (ksi)	0.2% Yield Strength (ksi)	Elongation (%)
Room	113.9	71	48.2
1000	88.7	62.8	34.8
1600	44.7	39.6	45.4

Table 4.3.2 Room temperature tensile data for HAYNES 230 alloy plate GTAW weldments made using 230-W filler metal (Ref. 33)

Material Condition	Ultimate Tensile Strength (ksi)	0.2% Yield Strength (ksi)	Elongation (%)	Fracture Site
As-Received	117.7	60.2	29.6	Weld
	113.4	58.4	28.2	Weld
Exposed at 1600F/1500 hrs.	123.8	57.5	24.9	Base
	120.9	58.8	23.6	Base
Exposed at 1600F/1500 hrs. + 2150F/0.5 hr./RAC	122.1	61.2	32.2	Base
	119.7	61.5	29.4	Weld